TABLE 1
RT-PCR primers used in this study

hAT1R, upper: 5′-GGC CAG TGT TTT TCT TTT GAA TTT AGC AC
hAT1R, lower: 5′-TGA ACA ATA GCC AGG TAT CGA TCA ATG C
hAT2R, upper: 5′-GTT CCC CTT GTT TGG TGT AT
hAT2R, lower: 5′-CAT CTT CAG GAC TTG GTC AC
mAT1R, upper: 5′-GCA TCA TCT TTG TGG TGG G
mAT1R, lower: 5′-GAA GAA AAG CAC AAT CGC C
mAT1aR, upper: 5′-GCA TCA TCT TTG TGG TGG G
mAT1aR, lower: 5′-ATC AGC ACA TCC AGG AAT G
mAT1bR, upper: 5′-GCATCATCTTTGTGG TGGG
mAT1bR, lower: 5′-ATG AGC ACA TCC AGA AAA C
mAT2R, upper: 5′-AGT GCA TGC GGG AGC TG
mAT2R, lower: 5′-GAC AAC AAA ACA GTG AG

mal human dermal fibroblasts were isolated from normal human skin and cultured in Dulbecco's modified Eagle's medium (DMEM; Invitrogen) supplemented with 10% fetal calf serum (FCS). Fourth- or fifth-passage cells were used. Mouse dermal fibroblasts were isolated from neonatal wild-type and AT1aR−/− mice and cultured in DMEM/10% FCS. Fourth-passage cells were used. Recombinant Ang II, PD123319, and CRM197 were purchased from Sigma. Valsartan, an AT1 receptor-selective blocker, was provided by Novartis Pharma AG (Basel, Switzerland). Anti-HB-EGF neutralizing antibody was purchased from R&D Systems (Tokyo, Japan). GM6001 and AG1478 were purchased from Calbiochem.

RT-PCR—Total RNA was extracted from cultured keratinocytes and fibroblasts using ISOGEN (Nippon Gene, Tokyo, Japan). Human AT1R and AT2R mRNAs and mouse AT1aR, AT1bR, and AT2R mRNAs were analyzed by RT-PCR using the primers listed in Table 1. RT-PCR was performed using RT-PCR High Plus (Toyobo Co., Ltd, Osaka, Japan) according to the manufacturer's instructions. The cDNA was reverse-transcribed from total RNA for 30 min at 60 °C and was heated to 94 °C for 2 min. The amplification was performed using a DNA thermal cycler (Astec, Fukuoka, Japan) for 25 cycles of denaturation for 1 min at 94 °C and annealing and primer extension for 1.5 min at 60 °C.

Migration Assay—Migration was evaluated using a modified Boyden chamber assay, as described previously (23). Briefly, a Nucleopore polyvinylpyrrolidine-free polycarbonate filter (8 μm; Neuro Probe, Inc., Gaithersburg, MD) was coated with type I collagen (Nitta Gelatin, Tokyo, Japan) for 30 min at room temperature and allowed to air dry. The filter was placed over a 48-well chamber containing various concentrations of Ang II in MCDB 153 without bovine pituitary extract for keratinocytes and in DMEM/2% FCS for fibroblasts. After trypsinization, 1×10^4 cells in 50 μl of serum-free MCDB 153 or DMEM were added to the wells in the upper chamber. The chamber was then placed in a humidified incubator at 37 °C for 7 h, after which the upper surface of the filter was scraped to remove non-migratory cells. The filter was subsequently fixed in buffered formalin for 30 min, washed with phosphate-buffered saline, and stained with hematoxylin and eosin. The total number of cells per well was counted by microscopy.

Proliferation Assay—Keratinocytes or fibroblasts were seeded on 6-well plates (5×10^4 cells/well). Next day, medium was replaced to basal medium (MCDB 153 for keratinocytes, DMEM/2% FCS for fibroblasts), and various concentrations of Ang II were added to the medium. After 4 days cell number was counted using Coulter Counter (Z1, Coulter).

Western Blot Analysis—Cells were harvested by scraping with extraction buffer containing 150 mM NaCl, 1% Nonidet P-40, 0.5% deoxycholate, 0.1% SDS, 50 mM Tris-HCl (pH 7.4), and protease inhibitors. Equal amounts of protein were separated by SDS-PAGE and transferred to polyvinylidene difluoride membranes. Primary antibodies (anti-EGFR and anti-phospho-EGFR; Transduction Laboratories, Lexington, KY) were incubated with the membranes at 4 °C overnight. Fluorescein-labeled goat anti-mouse or anti-rabbit IgG (GE Healthcare Biosciences Corp.) was used as the secondary antibody. The signal was amplified with an anti-fluorescein antibody followed by a fluorescent substrate, AttoPhos (GE Healthcare Biosciences Corp.). The membrane was scanned using FluoroImager (GE Healthcare Biosciences Corp.), and each band intensity was quantified with ImageQuant™ (GE Healthcare Biosciences Corp.). The control signal was defined as one unit.

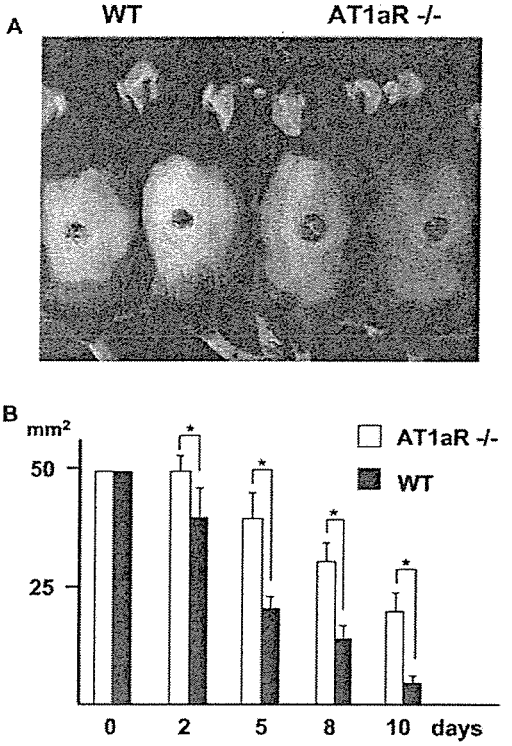

FIGURE 1. **Wound healing assay in AT1aR−/− mice.** An 8-mm punch biopsy was made in the back skin of 8-week-old female wild-type (*WT*) mice and AT1aR−/− mice, and wound closure was monitored. *A*, macroscopic view of wound healing on day 5. *B*, wound area measurement. *, $p < 0.05$.

AT1aR Knock-out Mice—AT1aR knock-out (AT1aR−/−) mice (based on C57BL/6J strain) (24) and wild-type mice were donated by Tanabe Seiyaku Co. Ltd., Osaka, Japan. The Animal Studies Committee of Ehime University approved the following experimental protocol.

Wound Healing Assay—Full-thickness, 8-mm punch biopsy wounds were made on the backs of 8-week-old female C57BL/6 wild-type mice and AT1aR−/− mice ($n = 6$). The edges of the wound were traced onto a clear film immediately after wounding. After treatment, the wounds were covered with a semipermeable polyurethane dressing. Wound areas were measured on days 0, 2, 5, 8, and 10.

Statistical Analysis—The results are representative of three independent experiments. p values were calculated using a two-sided Student's t test (see Figs. 1, 3, 4, 6, and 7; *NS*, not significant; *, $p < 0.05$).

RESULTS

Wound Healing in the AT1aR−/− Mouse—The *in vivo* function of Ang II was investigated in AT1aR knock-out mice. Full-thickness, 8-mm round wounds were prepared on the backs of 8-week-old female C57BL/6 wild-type mice and AT1aR−/− mice. In wild-type mice, the wound areas had decreased to 80% their original size by day 2, but the wound areas were unchanged in AT1aR−/− mice. On day 5, the wound areas were about 50% their original size in wild-type mice but 80% in

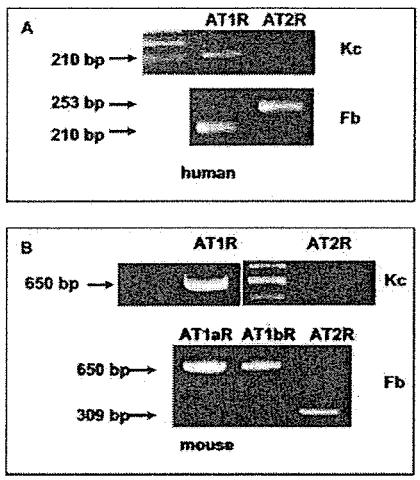

FIGURE 2. **Angiotensin II receptor expression in keratinocytes and fibroblasts.** Angiotensin II receptor expression was analyzed by RT-PCR. *A*, human; *B*, mouse. *Kc*, keratinocyte; *Fb*, fibroblast.

AT1aR−/− mice (Fig. 1*A*). On day 10, the wounds of wild-type mice were almost healed, whereas the wounds of AT1aR−/− mice were still about 50% their initial size. The differences in wound healing between wild-type and AT1aR−/− mice from day 2 to day 10 were significant (Fig. 1*B*). These results indicate that Ang II plays an important role in cutaneous wound healing.

Ang II Receptor Expression in Cultured Skin Keratinocytes and Fibroblasts—Keratinocytes and fibroblasts are the major cells responsible for cutaneous wound healing. We therefore examined which type of Ang II receptors are expressed in cultured human keratinocytes and fibroblasts. RT-PCR demonstrated that keratinocytes expressed AT1R but not AT2R mRNA, whereas fibroblasts expressed mRNA of both AT1R and AT2R (Fig. 2*A*). In cultured mouse keratinocytes, AT1R, but not AT2R, was expressed, while in mouse fibroblasts AT1aR, AT1bR, and AT2R were detected (Fig. 2*B*). These results demonstrate that Ang II receptors are expressed differentially depending on the cell type.

Angiotensin II-induced Keratinocyte and Fibroblast Proliferation and Migration—As cell migration and cell proliferation play central roles in cutaneous wound healing, first we examined the effect of Ang II on cell

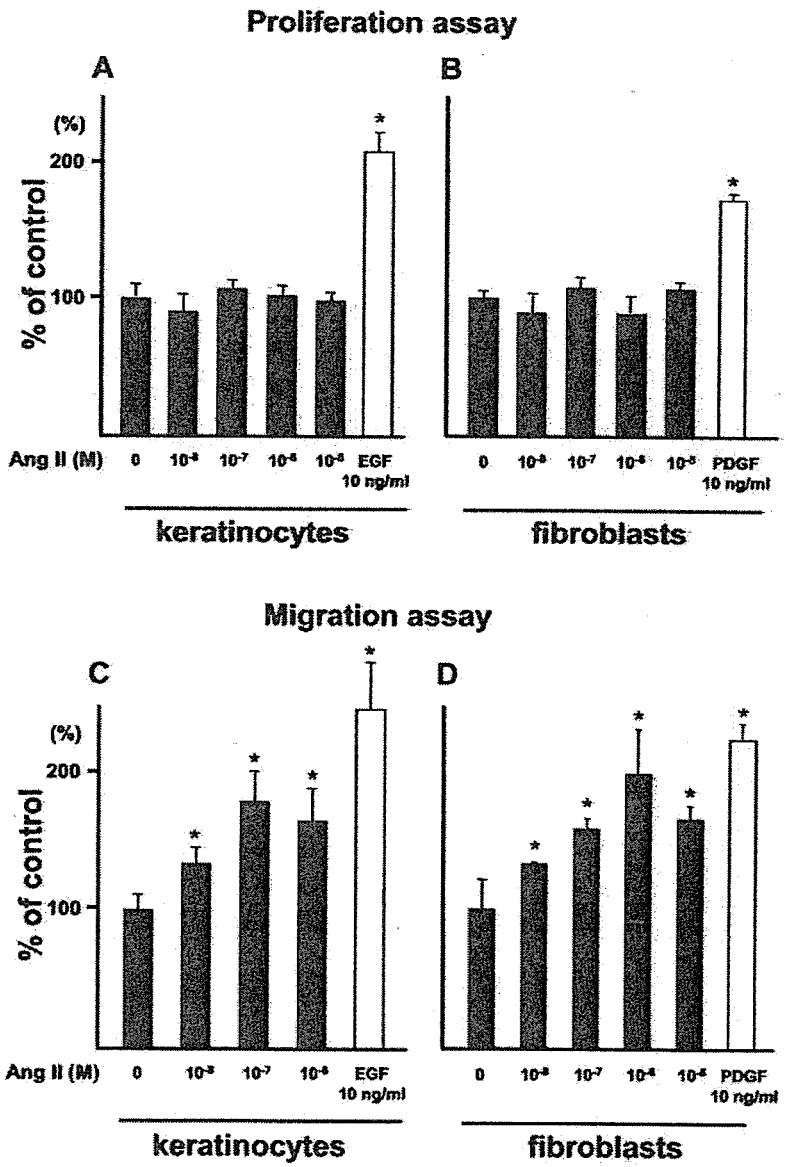

FIGURE 3. **Proliferation and migration of keratinocytes and fibroblasts induced by angiotensin II.** Proliferation was examined by growth assay. Keratinocytes or fibroblasts were seeded on 6-well plates (5×10^4 cells/well), and various concentrations of Ang II were added to the medium. After 4 days cell number was counted using Coulter Counter (Z1, Coulter). *A*, keratinocytes; *B*, fibroblasts. Migration was assessed by a Boyden chamber assay. *C*, Ang II induced keratinocyte migration by a maximum of 1.7-fold at 10^{-7} M. EGF was used as a positive control. *D*, Ang II induced fibroblast migration by a maximum of 2.0-fold at 10^{-7} M. PDGF was used as a positive control. *, $p < 0.05$.

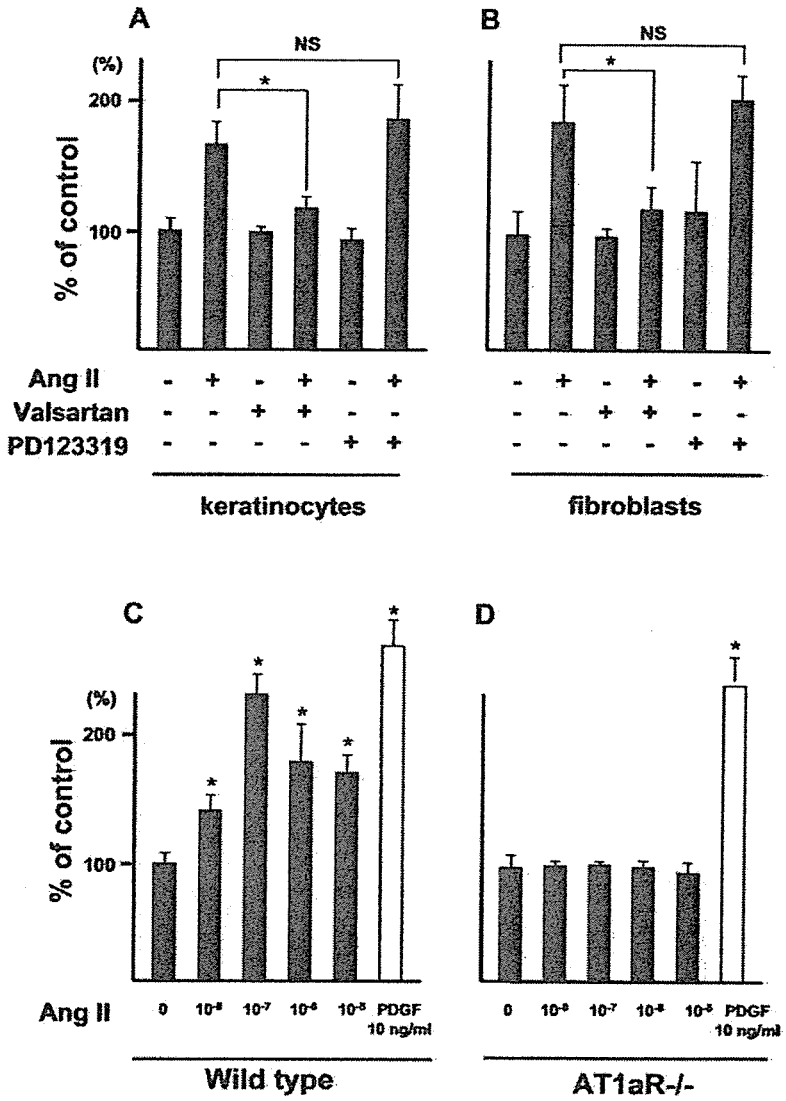

FIGURE 4. **Role of angiotensin II receptors on angiotensin II-induced migration.** Valsartan (AT1R antagonist) or PD123319 (AT2R antagonist) was added to the medium, and Ang II-induced migration was assessed by a Boyden chamber assay. *A*, keratinocytes; *B*, fibroblasts. *, $p < 0.05$; *NS*, not significant. Fibroblasts were prepared from wild-type (*C*) and AT1aR−/− (*D*) mice, and Ang II-induced migration was examined. PDGF was used as a positive control. *, $p < 0.05$.

proliferation. Keratinocytes and fibroblasts were seeded on 6-well plates (5×10^4 cells/well), and various concentrations of Ang II (1×10^{-8} to 10^{-5} M) were added to the medium. After 4 days incubation, cell number was counted. Ang II did not promote cell proliferation of both type of cells (Fig. 3, *A* and *B*). Next the effect of Ang II on the migration of keratinocytes and fibroblasts was examined. Human keratinocytes and fibroblasts were seeded on type I collagen-coated filters, and various concentrations of Ang II were added to the medium. After 7 h, Ang II enhanced keratinocyte migration in a dose-dependent manner, by a maximum of 1.7-fold at 10^{-7} M compared with control (Fig. 3*C*). Ang II also enhanced fibroblast migration by a maximum of 2.0-fold at 10^{-7} M compared with control (Fig. 3*D*). Therefore, Ang II at a concentration of 10^{-7} M was used to stimulate keratinocytes and fibroblasts in the following experiments.

The effect of AT1R and AT2R inhibitors on Ang II-induced keratinocyte and fibroblast migration was investigated. Valsartan, a specific inhibitor for AT1R, inhibited Ang II-induced keratinocyte migration by 80%. As expected, PD123319, a specific inhibitor for AT2R, did not inhibit Ang II-induced keratinocyte migration (Fig. 4*A*) because these cells lack this receptor. Similar to the results in keratinocytes, valsartan inhibited Ang II-induced fibroblast migration by 76%, whereas PD123319 did not prevent Ang II-induced fibroblast migration (Fig. 4*B*). We further confirmed that Ang II-induced migration was mediated via AT1R signaling using fibroblast prepared from wild-type and AT1aR−/− mice. Ang II enhanced fibroblast migration by a maximum of 2.3-fold at 10^{-7} M in wild type mice (Fig. 4*C*), whereas it did not enhance migration of AT1aR−/− fibroblasts (Fig. 4*D*). These results indicate that Ang II-induced migration is mediated through AT1R signaling.

A Role for HB-EGF-mediated EGFR Transactivation in Ang II-induced Cell Migration—Recent studies demonstrated that the stimulation of GPCR induces the shedding of EGFs via ADAM, with subsequent transactivation of EGFR. It is well known that EGFR activation triggers cell migration (25). As AT1R is a GPCR, the phosphorylation of EGFR in response to stimulation with Ang II was investigated in both cell types. EGFR was phosphorylated 5–15 min after the addition of Ang II in keratinocytes, and Ang II-induced EGFR phosphorylation was completely blocked by pre-treatment with valsartan (Fig. 5*A*). In fibroblasts, the amount of phosphorylated EGFR was increased remarkably 30 min after the addition of Ang II, and phosphorylation was completely suppressed by valsartan (Fig. 5*B*). The AT2R blocker PD123319 did not affect Ang II-induced EGFR phosphorylation (data not shown).

The role of HB-EGF in Ang II-induced cell migration was determined by assaying keratinocyte and fibroblast migration using an anti-HB-EGF antibody. Pretreatment with the anti-HB-EGF antibody inhibited Ang II-induced keratinocyte and fibroblast migration by 100 and 48%, respectively. (Fig. 6, *A* and *B*). The effect of HB-EGF on Ang II-induced migration was further confirmed using CRM197, a non-toxic mutant of diphtheria toxin that selectively binds and inactivates HB-EGF. The addition of CRM197 into the medium inhibited Ang II-induced keratinocyte migration by 45% (Fig. 6*C*) and Ang II-induced fibroblast migration by 80% compared with controls (Fig. 6*D*).

Finally we investigated the effects of MMP inhibitor and ErbB inhibitor on Ang II-induced migration. Treatment with ErbB kinase inhibitor (AG1478; 30 nM) inhibited Ang II-induced keratinocyte and fibroblast migration completely. (Fig. 7*A*, B). The addition of GM6001 (MMP inhibitor) into the medium inhibited Ang II-induced keratinocyte migration by 65% (Fig. 7*C*) and Ang II-induced fibroblast migration by 90% compared with controls (Fig. 7*D*). These results indicated that Ang II-induced keratinocyte and fibroblast migration is mediated through EGFR transactivation, mainly by HB-EGF shedding.

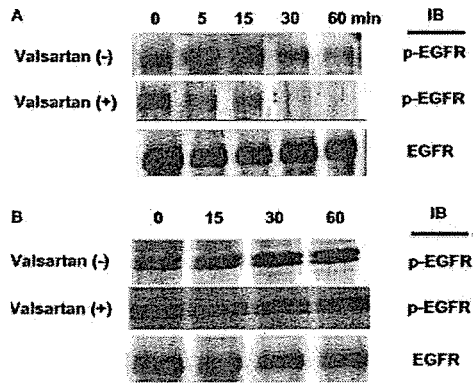

FIGURE 5. **Effects of AT1R antagonist (valsartan) on angiotensin II-induced EGFR phosphorylation.** After the addition of valsartan (AT1R antagonist) to the medium, Ang II-induced EGFR phosphorylation was analyzed by Western blot. *A*, keratinocytes; *B*, fibroblasts. *p-EGFR*, anti-phospho-EGFR antibody.

DISCUSSION

The results of this study demonstrate that Ang II promotes cutaneous wound healing. While it has long been recognized that growth factors participate in cutaneous wound healing, it is remarkable that Ang II, which plays a role in the control of systemic blood pressure and volume homeostasis, is also involved in wound healing. Previous studies have shown that Ang II affects many aspects of wound repair, including cellular proliferation, chemotaxis, extracellular matrix production, and angiogenesis (20).

It has been reported that adult rat skin contains predominantly AT1R (18) and that Ang II accelerates the closure of thermal injuries and full-thickness dermal lesions in these animals. In addition to the contribution of exogenous Ang II to wound repair, studies have shown that increased levels of Ang II and ATRs are produced at the site of wound

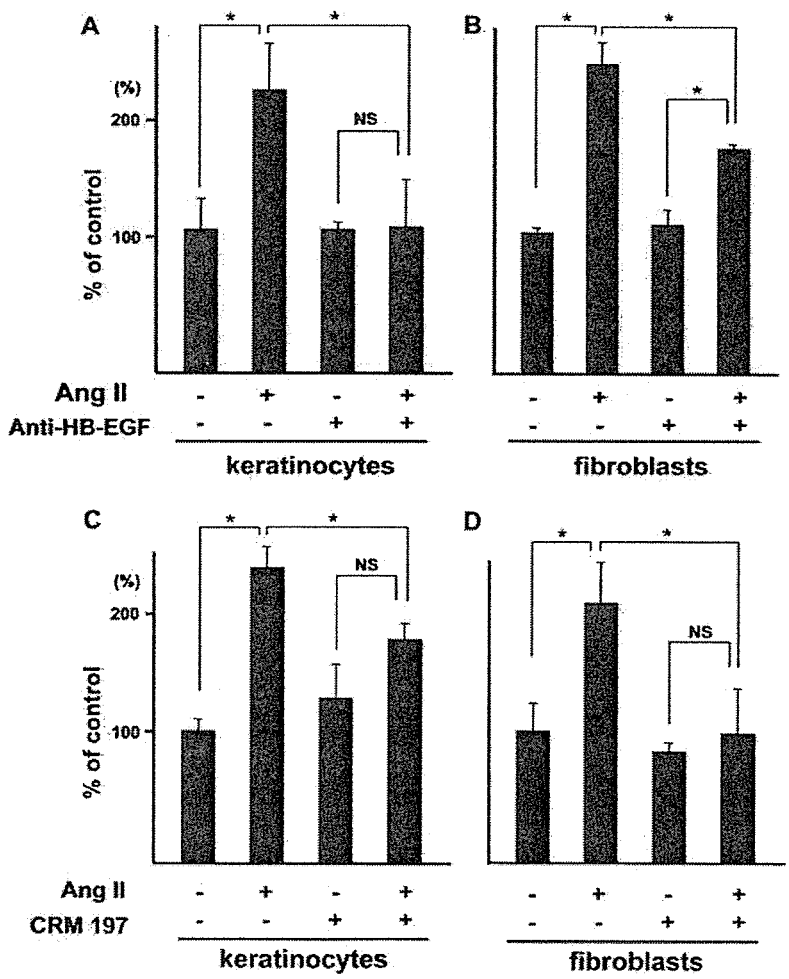

FIGURE 6. **Effects of anti-HB-EGF neutralizing antibody and CRM197 on angiotensin II-induced migration.** Anti-HB-EGF neutralizing antibody was added to the medium, after which Ang II-induced migration was assessed by a Boyden chamber assay. *A*, keratinocytes; *B*, fibroblasts. CRM197 (diphtheria toxin mutant; HB-EGF inactivator) was added to the medium, and Ang II-induced migration was assessed by a Boyden chamber assay. *C*, keratinocytes; *D*, fibroblasts. *, $p < 0.05$; *NS*, not significant.

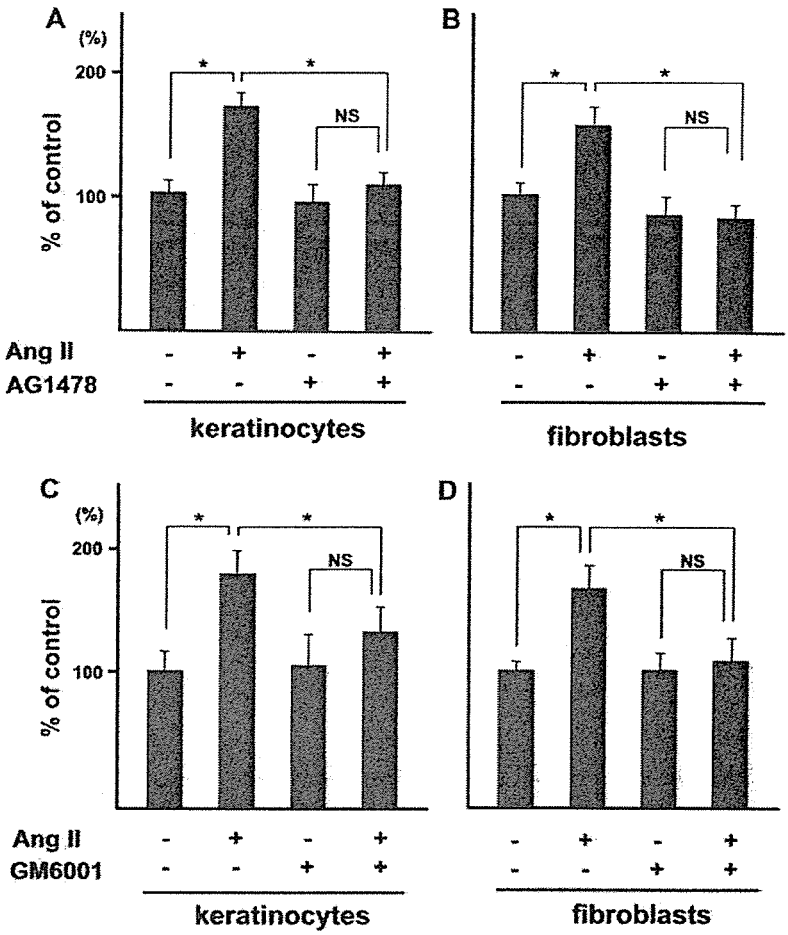

FIGURE 7. **Effects of MMP inhibitor and ErbB inhibitor on angiotensin II-induced migration.** MMP inhibitor (GM6001; 50 μM) or ErbB kinase inhibitor (AG1478; 30 nM) was added to the medium, after which Ang II-induced migration was assessed by a Boyden chamber assay. *A*, AG1478/keratinocytes; *B*, AG1478/fibroblasts; *C*, GM6001/keratinocytes; *D*, GM6001/fibroblasts. *, $p < 0.05$; *NS*, not significant.

repair (18–21). Takeda *et al.* (26) studied the effect of Ang II on skin wound healing and found that it is regulated by the balance of AT1R and AT2R and that the induction of AT1R signaling accelerated keratinocyte re-epithelization and myofibroblast recovery. These reports led us to investigate the role of Ang II in skin wound healing and its mechanisms. Using AT1aR knock-out mice, we were able to show, for the first time, that Ang II is involved in cutaneous wound healing.

Skin wound healing is a complex process requiring several coordinated events, including inflammation, cell migration, cell proliferation, matrix production, and angiogenesis (1), and it involves a complex array of cells, growth factors, cytokines, and matrix components. Members of the EGF family are the most important growth factors related to epithelialization during cutaneous wound healing. Among the EGF family members, TGF-α, HB-EGF, amphiregulin, and epiregulin are autocrine growth factors produced by epidermal keratinocytes (27–30). No differences were found in the healing of either excisional dorsal wounds or ear-punch wounds between TGF-α knock-out mice and wild-type mice (31, 32). Epiregulin knock-out mice also did not show any delay in wound healing (33). The absence of an effect on wound healing in EGFR-ligand knock-out mice is probably attributable to the known functional redundancy among EGF family members. Recently, we used keratinocyte-specific-HB-EGF knock-out mice to demonstrate that HB-EGF enhances keratinocyte migration and is thus an important growth factor in skin wound healing (34). HB-EGF binds to ErbB1 and ErbB4 (35). ErbB1 knock-out mice do not exhibit impaired wound healing (36). Together, ErbB4 signaling from HB-EGF in skin wound healing should be clarified in future.

As not only proliferation but also cellular migration are essential to wound healing, the effect of Ang II on cell migration was examined. We demonstrated that the major determinant of accelerated cutaneous wound repair by Ang II is increased keratinocyte and fibroblast migration. In further experiments, cross-talk between Ang II and EGF family members, especially HB-EGF, was studied. Ang II is known to induce EGFR phosphorylation, a process referred to as EGFR transactivation. EGFR transactivation by GPCR agonists was initially thought to be independent of EGFR ligands and achieved solely by intracellular events. This interpretation was based on the rapid onset of EGFR phosphorylation as well as an apparent lack of EGFR ligands in the conditioned media of cells stimulated with GPCR agonists (37). GPCRs employ multiple distinct pathways to activate the extracellular signal-regulated kinase/mitogen-activated protein kinase (ERK/MAPK) cascade. It has been reported that GPCR-stimulated tyrosine phosphorylation of EGFR involves the release of a soluble EGFR ligand, HB-EGF (38). HB-EGF is proteolytically cleaved at a juxtamembrane site, leading to the shedding of soluble HB-EGF, which activates EGFR in an autocrine/paracrine manner (17). We previously reported that that shedding of EGFR ligands represents a critical event in keratinocyte migration and the early phases of wound healing (23).

Based on these observations, we examined how transactivation is involved in Ang II-induced keratinocyte and fibroblast migration. Our results confirm that Ang II induces EGFR phosphorylation in both keratinocytes and fibroblasts, with maximal activation occurring within 15 and 30 min, respectively. Ang II-induced cell migration was found to be inhibited by ErbB kinase inhibitor, HB-EGF neutralizing antibody, and

CRM197, which indicates that Ang II-induced cell migration is mediated mainly by HB-EGF shedding through AT1R.

There have been several reports describing the role of metalloproteases in mediating EGFR transactivation and the subsequent functions induced by many GPCRs. Asakura *et al.* (39) reported that cellular signaling in cardiomyocytes following treatment with GPCR agonists is dependent upon EGFR transactivation triggered by ADAM 12-mediated cleavage of HB-EGF. Mifune *et al.* (40) concluded that Ang II stimulates ADAM 17-dependent HB-EGF shedding through AT1R in COS-7 cells. In this study, broad spectrum MMP inhibitor (GM6001) inhibited Ang II-induced migration, which suggests that shedding of EGF ligands was critical in these events. Given that different types of cells were used in these experiments, the metalloprotease responsible for HB-EGF shedding may depend on the particular cells and organs.

Our observation led to an interesting clinical question: is cutaneous wound healing delayed in individuals receiving AT1R antagonists to treat hypertension? Drug dosage information shows that the blood level of AT1R antagonist is lower than the dose used in our research. Takeda *et al.* (26) reported the effect of the AT1 blocker candesartan on re-epithelization and vascular growth in a rat *in vivo* model. The group receiving candesartan (10 mg/kg/day) showed delayed re-epithelization and dermal repair as well as a suppression of angiogenesis. However, in animals given 1 mg of candesartan/kg/day, angiogenesis was only slightly suppressed, and re-epithelization of the wounds was observed on day 12 after wounding. This result was almost the same as the control. A typical human dose of AT1R antagonist is ~1 mg/kg/day, and thus wound healing should not be delayed in persons taking these drugs.

Takeda *et al.* (26) reported that bromodeoxyuridine incorporation into keratinocytes and myofibroblasts is enhanced via AT1R signaling and suppressed via AT2R signaling and that the recovery of keratinocytes and myofibroblasts in migration assays is accelerated by AT1R signaling but inhibited by AT2R signaling. Most of the known biological effects of Ang II are mediated through AT1R. We therefore examined Ang II receptor expression in keratinocytes and fibroblasts, which are the main cell types contributing to skin wound healing. AT1R was expressed in both human and mouse keratinocytes and fibroblasts, whereas AT2R was detected only in human and mouse fibroblasts. Recombinant Ang II enhanced the migration of keratinocytes and fibroblasts *in vitro*, while migration was inhibited by the AT1R-specific inhibitor valsartan. By contrast, neither keratinocyte nor fibroblast migration was inhibited by the AT2R blocker PD123319. These results indicated that Ang II-induced keratinocyte and fibroblast migration is mediated by AT1R.

Ang II has been shown to enhance growth factor production in fibroblasts, and several studies implicate Ang II in cardiac fibrosis because of stimulated fibroblast proliferation (41). However, these effects could result in part from the paracrine actions of growth factors from Ang II-stimulated fibroblasts. Indeed, the inhibition of fibroblast proliferation in cultures of neonatal cardiac cells reduces Ang II-induced protein synthesis in cardiomyocytes (42). A recent study demonstrated the importance of AT1R-expressing cardiomyocytes in the proliferative response of cardiac fibroblasts to Ang II (43). Ang II, via AT1R, also appears to up-regulate FGF-2 expression in cardiac myocytes (44). We found that Ang II-induced migration and EGFR activation are mediated via AT1R signaling in epidermal keratinocytes and dermal fibroblasts. Our result of delayed wound healing in AT1aR−/− mice is consistent with this observation.

The regulation of collagen synthesis is an important part of Ang II-induced wound healing (45, 46). Collagen homeostasis is regulated by a delicate dynamic balance of synthesis and degradation. The crucial role of collagen synthesis in dermal wound repair is well understood, and Ang II has been demonstrated to be closely associated with the production of extracellular matrix. In skin, fibroblasts are pivotal for collagen production, and numerous collagenous structures need to be reconstituted after injury. Recently we have reported that Ang II increased collagen production via AT1R but inhibited collagen production via AT2R in mouse neonatal skin fibroblasts and that AT1aR−/− fibroblasts showed decreased collagen production (47). The decreased collagen production as well as impaired cell migration in AT1aR−/− mice plays an important role in delayed wound healing in these mice. Moreover, AT1R activation led to enhancement of insulin-like growth factor-I-induced collagen synthesis (47). The regulation of collagen production by the antagonistic actions of AT1R and AT2R in skin fibroblasts also supports the pathophysiological significance of Ang II in the skin. A detailed analysis of the specific cell types expressing AT1R and AT2R and their localization in the process of skin wound healing is necessary for understanding the complete role of Ang II in cutaneous wound healing.

In conclusion, we have demonstrated for the first time that Ang II plays an important role in skin wound healing *in vitro* and *in vivo* and that it functions by accelerating both keratinocyte and fibroblast migration in a process mediated by HB-EGF shedding.

Acknowledgment—We thank Eriko Tan for excellent technical assistance.

REFERENCES

1. Singer, A. J., and Clark, R. A. (1999) *N. Engl. J. Med.* **341,** 738–746
2. Hashimoto, K. (2000) *J. Dermatol. Sci.* **24,** Suppl. 1, S46–S550
3. Crabos, M., Roth, M., Hahn, A. W., and Erne, P. (1994) *J. Clin. Invest.* **93,** 2372–2378
4. Sun, Y., Diaz-Arias, A. A., and Weber, K. T. (1994) *J. Lab. Clin. Med.* **123,** 372–377
5. Campbell-Boswell, M., and Robertson, A. L., Jr. (1981) *Exp. Mol. Pathol.* **35,** 265–276
6. Daemen, M. J., Lombardi, D. M., Bosman, F. T., and Schwartz, S. M. (1991) *Circ. Res.* **68,** 450–456
7. Owens, G. K. (1985) *Circ. Res.* **56,** 525–536
8. Paquet, J. L., Baudouin-Legros, M., Brunelle, G., and Meyer, P. (1990) *J. Hypertens.* **8,** 565–572
9. Schelling, P., Ganten, D., Speck, G., and Fischer, H. (1979) *J. Cell Physiol.* **98,** 503–513
10. Schorb, W., Conrad, K. M., Singer, H. A., Dostal, D. E., and Baker, K. M. (1995) *J. Mol. Cell. Cardiol.* **27,** 1151–1160
11. Timmermans, P. B., Wong, P. C., Chiu, A. T., Herblin, W. F., Benfield, P., Carini, D. J., Lee, R. J., Wexler, R. R., Saye, J. A., and Smith, R. D. (1993) *Pharmacol. Rev.* **45,** 205–251
12. Hahn, A. W., Resink, T. J., Kern, F., and Buhler, F. R. (1993) *J. Cardiovasc. Pharmacol.* **22,** Suppl. 5, S37–S43
13. Ko, Y., Stiebler, H., Nickenig, G., Wieczorek, A. J., Vetter, H., and Sachinidis, A. (1993) *Am. J. Hypertens.* **6,** 496–499
14. Ohkubo, N., Matsubara, H., Nozawa, Y., Mori, Y., Murasawa, S., Kijima, K., Maruyama, K., Masaki, H., Tsutumi, Y., Shibazaki, Y., Iwasaka, T., and Inada, M. (1997) *Circulation* **96,** 3954–3962
15. Tsuzuki, S., Matoba, T., Eguchi, S., and Inagami, T. (1996) *Hypertension* **28,** 916–918
16. Yamada, T., Horiuchi, M., and Dzau, V. J. (1996) *Proc. Natl. Acad. Sci. U. S. A.* **93,** 156–160
17. Raab, G., and Klagsbrun, M. (1997) *Biochim. Biophys. Acta* **1333,** F179–F199
18. Kimura, B., Sumners, C., and Phillips, M. I. (1992) *Biochem. Biophys. Res. Commun.* **187,** 1083–1090
19. Okuyama, N., Roda, N., Sherman, R., Guerrero, A., Dougherty, W., Nguyen, T., diZerega, G., and Rodgers, K. (1999) *Ann. Plast. Surg.* **42,** 313–319
20. Rodgers, K., Xiong, S., Felix, J., Roda, N., Espinoza, T., Maldonado, S., and Dizerega, G. (2001) *Wound Repair Regen.* **9,** 238–247
21. Rodgers, K. E., DeCherney, A. H., St Amand, K. M., Dougherty, W. R., Felix, J. C., Girgis, W. W., and diZerega, G. S. (1997) *J. Burn Care Rehabil.* **18,** 381–388
22. Shirakata, Y., Ueno, H., Hanakawa, Y., Kameda, K., Yamasaki, K., Tokumaru, S., Yahata, Y., Tohyama, M., Sayama, K., and Hashimoto, K. (2004) *J. Dermatol. Sci.* **36,** 41–50
23. Tokumaru, S., Higashiyama, S., Endo, T., Nakagawa, T., Miyagawa, J. I., Yamamori, K., Hanakawa, Y., Ohmoto, H., Yoshino, K., Shirakata, Y., Matsuzawa, Y., Hashimoto, K., and Taniguchi, N. (2000) *J. Cell Biol.* **151,** 209–220
24. Sugaya, T., Nishimatsu, S., Tanimoto, K., Takimoto, E., Yamagishi, T., Imamura, K.,

Goto, S., Imaizumi, K., Hisada, Y., Otsuka, A., and Uchida, H., Sugiura, M., Fukuta, K., Fukamizu, A., and Murakami, K. (1995) *J. Biol. Chem.* **270,** 18719–18722
25. Barrandon, Y., and Green, H. (1987) *Cell* **50,** 1131–1137
26. Takeda, H., Katagata, Y., Hozumi, Y., and Kondo, S. (2004) *Am. J. Pathol.* **165,** 1653–1662
27. Coffey, R. J., Jr., Derynck, R., Wilcox, J. N., Bringman, T. S., Goustin, A. S., Moses, H. L., and Pittelkow, M. R. (1987) *Nature* **328,** 817–820
28. Cook, P. W., Mattox, P. A., Keeble, W. W., Pittelkow, M. R., Plowman, G. D., Shoyab, M., Adelman, J. P., and Shipley, G. D. (1991) *Mol. Cell. Biol.* **11,** 2547–2557
29. Hashimoto, K., Higashiyama, S., Asada, H., Hashimura, E., Kobayashi, T., Sudo, K., Nakagawa, T., Damm, D., Yoshikawa, K., and Taniguchi, N. (1994) *J. Biol. Chem.* **269,** 20060–20066
30. Shirakata, Y., Komurasaki, T., Toyoda, H., Hanakawa, Y., Yamasaki, K., Tokumaru, S., Sayama, K., and Hashimoto, K. (2000) *J. Biol. Chem.* **275,** 5748–5753
31. Luetteke, N. C., Qiu, T. H., Peiffer, R. L., Oliver, P., Smithies, O., and Lee, D. C. (1993) *Cell* **73,** 263–278
32. Mann, G. B., Fowler, K. J., Gabriel, A., Nice, E. C., Williams, R. L., and Dunn, A. R. (1993) *Cell* **73,** 249–261
33. Shirasawa, S., Sugiyama, S., Baba, I., Inokuchi, J., Sekine, S., Ogino, K., Kawamura, Y., Dohi, T., Fujimoto, M., and Sasazuki, T. (2004) *Proc. Natl. Acad. Sci. U. S. A.* **101,** 13921–13926
34. Shirakata, Y., Kimura, R., Nanba, D., Iwamoto, R., Tokumaru, S., Morimoto, C., Yokota, K., Nakamura, M., Sayama, K., Mekada, E., Higashiyama, S., and Hashimoto, K. (2005) *J. Cell Sci.* **118,** 2363–2370
35. Harris, R. C., Chung, E., and Coffey, R. J. (2003) *Exp. Cell Res.* **284,** 2–13
36. Hansen, L. A., Alexander, N., Hogan, M. E., Sundberg, J. P., Dlugosz, A., Threadgill, D. W., Magnuson, T., and Yuspa, S. H. (1997) *Am. J. Pathol.* **150,** 1959–1975
37. Uchiyama-Tanaka, Y., Matsubara, H., Nozawa, Y., Murasawa, S., Mori, Y., Kosaki, A., Maruyama, K., Masaki, H., Shibasaki, Y., Fujiyama, S., Nose, A., Iba, O., Hasagawa, T., Tateishi, E., Higashiyama, S., and Iwasaka, T. (2001) *Kidney Int.* **60,** 2153–2163
38. Prenzel, N., Zwick, E., Daub, H., Leserer, M., Abraham, R., Wallasch, C., and Ullrich, A. (1999) *Nature* **402,** 884–888
39. Asakura, M., Kitakaze, M., Takashima, S., Liao, Y., Ishikura, F., Yoshinaka, T., Ohmoto, H., Node, K., Yoshino, K., Ishiguro, H., Asanuma, H., Sanada, S., Matsumura, Y., Takeda, H., Beppu, S., Tada, M., Hori, M., and Higashiyama, S. (2002) *Nat. Med.* **8,** 35–40
40. Mifune, M., Ohtsu, H., Suzuki, H., Nakashima, H., Brailoiu, E., Dun, N. J., Frank, G. D., Inagami, T., Higashiyama, S., Thomas, W. G., Eckhart, A. D., Dempsey, P. J., and Eguchi, S. (2005) *J. Biol. Chem.* **280,** 26592–26599
41. Booz, G. W., and Baker, K. M. (1995) *Cardiovasc. Res.* **30,** 537–543
42. Kim, N. N., Villarreal, F. J., Printz, M. P., Lee, A. A., and Dillmann, W. H. (1995) *Am. J. Physiol.* **269,** E426–E437
43. Matsusaka, T., Katori, H., Inagami, T., Fogo, A., and Ichikawa, I. (1999) *J. Clin. Invest.* **103,** 1451–1458
44. Fischer, T. A., Ungureanu-Longrois, D., Singh, K., de Zengotita, J., DeUgarte, D., Alali, A., Gadbut, A. P., Lee, M. A., Balligand, J. L., Kifor, I., Smith, T. W., and Kelly, R. A. (1997) *Am. J. Physiol.* **272,** H958–H968
45. Laurent, G. J. (1987) *Am. J. Physiol.* **252,** C1–C9
46. Lindblad, W. J. (1998) *Wound Repair. Regen.* **6,** 186–193
47. Min, L. J., Cui, T. X., Yahata, Y., Yamasaki, K., Shiuchi, T., Liu, H. W., Chen, R., Li, J. M., Okumura, M., Jinno, T., Wu, L., Iwai, M., Nahmias, C., Hashimoto, K., and Horiuchi, M. (2004) *Endocrinology* **145,** 253–260

Cell Tissue Res (2006) 326: 69–77
DOI 10.1007/s00441-006-0208-2

REGULAR ARTICLE

Lujun Yang · Yuji Shirakata · Masachika Shudou · Xiuju Dai · Sho Tokumaru · Satoshi Hirakawa · Koji Sayama · Junji Hamuro · Koji Hashimoto

New skin-equivalent model from de-epithelialized amnion membrane

Received: 14 December 2005 / Accepted: 23 March 2006 / Published online: 7 June 2006

Abstract The presence of pre-existing basement membrane (BM) components improves the morphogenesis of epidermis and BM in constructing a human living skin-equivalent (LSE). De-epithelialized amniotic membrane (AM) retains key BM components. We have therefore investigated the usefulness of AM for constructing LSE. De-epithelialized AM was overlaid on type I collagen gel embedded with fibroblasts. Normal human keratinocytes (NHKs) were then seeded onto the epithelial side of the AM to construct an AM-LSE. A conventional LSE was constructed by seeding NHKs on a fibroblast-populated type I collagen gel. When the keratinocytes reached confluence, the LSE was lifted to the air-liquid interface and cultured for up to 3 weeks. Samples were harvested at various times and investigated morphologically, immunohistochemically, and ultrastructurally. In AM-LSE, the epidermis was better stratified, with more compact, polarized, columnar basal cells, and the expression of differentiation and proliferation markers was more similar to that of normal human skin than was that of LSE without AM. A more continuous BM and better-developed hemidesmosomes were found in AM-LSE. The epidermis of AM-LSE outgrew much faster than that of LSE without AM. When transplanted onto nude mice, both LSEs took well; however, the AM-LSE graft showed better morphogenesis of the epidermis, BM, and hemidesmosomes. The better epidermal morphology and better-developed BM in AM-LSE in vitro and in vivo indicates its superiority over LSE without AM for clinical applications.

Keywords Amniotic membrane · Basement membrane · Keratinocyte · Migration · Skin-equivalent · Human · Mouse (BALB/cAJc1-nu)

This work was partly supported by Health Sciences Research Grants for Research on Specific Diseases from the Ministry of Health, Labor, and Welfare of Japan (to K.H.) and a Grant-in-Aid for Scientific Research from the Ministry of Education, Culture, Sports, Science, and Technology of Japan (to K.H. and Y.S.).
L. Yang and Y. Shirakata contributed equally to this work.

L. Yang · Y. Shirakata (✉) · X. Dai · S. Tokumaru · S. Hirakawa · K. Sayama · K. Hashimoto
Department of Dermatology,
Ehime University School of Medicine,
Shitsukawa,
Toon, Ehime 791-0295, Japan
e-mail: shirakat@m.ehime-u.ac.jp
Tel.: +81-89-9605350
Fax: +81-89-9605352

M. Shudou
Department of Bioscience, Ehime University,
Shitsukawa,
Toon, Ehime 791-0295, Japan

J. Hamuro
ArBlast,
Chuo-ku, Kobe 650-0047, Japan

Introduction

Living skin-equivalent (LSE), which consists of epidermis and dermis matrix, has long been used as a skin substitute for wound closure (Eaglstein and Falanga 1998). A well-developed differentiated epidermis provides a barrier against bacteria and other environmental factors, and the presence of a basement membrane (BM) and fibroblasts are necessary for maintaining epidermal architecture and sustaining growth (Andriani et al. 2003). A variety of biomaterials has been used to construct the dermal matrix of LSE (Guerret et al. 2003; Llames et al. 2004; Meana et al. 1998; Medalie et al. 1997; Ojeh et al. 2001), including type I collagen gel, fibrin gel, human plasma, and acellular human dermis. This shows that BM is not just an inert matrix that supports the epidermis, but that it also regulates epidermal morphogenesis and homeostasis via dynamic cross-talk with the overlying epidermis. Among dermal materials, acellular human dermis possesses an intact BM and supports the epidermis with good morphogenesis and a rete ridge-like pattern. The presence of pre-existing BM component proteins of the dermal matrix is essential for the development of the BM in an LSE (Ralston et al. 1999).

However, large amounts of human dermis are difficult to obtain for clinical application.

Amniotic membrane (AM) is composed of a single layer of columnar epithelial cells, a BM, an acellular compact layer, and the underlying fibroblast and spongy layers (von Versen-Hoynck et al. 2004). The BM zone underlying the amniotic epithelium resembles that of skin morphologically and ultrastructurally and consists of laminin 5 and types IV, VII, and XVII collagen (Oyama et al. 2003). As a biomaterial, AM is readily available and inexpensive and has been used to cover wounds temporarily, thereby reducing inflammation, facilitating epithelialization, and preventing scarring (Sheridan and Moreno 2001; Tseng 2001). De-epithelialized amnion has been employed as a carrier tissue for corneal or oral epithelial cell cultures to make a cornea-equivalent for ocular surface reconstruction (Nakamura et al. 2003a,b, 2004).

Since AM retains the major BM components, AM might be useful for constructing a better LSE. In this study, we have prepared de-epithelialized AM that retains the major BM components and have investigated whether AM improves the epidermis in an LSE. We have seeded keratinocytes onto AMs previously placed (epithelial side up) onto fibroblast-populated type I collagen gels, in order to construct an AM-LSE. Conventional LSEs have also been constructed from the same keratinocytes and fibroblasts by using the same protocol, except for the use of AM. We have further investigated the usefulness of AM for LSE in vitro and in vivo.

Materials and methods

Cell culture

Normal human epidermal keratinocytes (NHKs) were isolated from healthy human skin and cultured under serum-free conditions, as described previously (Shirakata et al. 2003, 2004). The cells were used for LSE cultures in their fourth passage. Fibroblasts were isolated from normal human skin and cultured in DMEM supplemented with 10% fetal calf serum (FCS), and 5th passage cells were used to construct the LSE. All procedures that involved human subjects received prior approval from the Ethics Committee of Ehime University School of Medicine, Toon, Ehime, Japan, and all subjects provided written informed consent.

Preparation of cultured skin-equivalents

The preparation of LSE has been described previously (Yang et al. 2005). Briefly, a collagen gel was prepared by mixing six volumes of ice-cold porcine collagen type I solution (Nitta Gelatin, Osaka, Japan) with one volume of 8×DMEM (Gibco), ten volumes of 1×DMEM supplemented with 20% FCS, and one volume of 0.1 N NaOH. Of this solution, 1 ml was added to each culture insert (Transwel-COL, membrane pore-size: 3 μm, Costar) in a 6-well culture plate (Costar). Following polymerization of the gel in the inserts at 37°C, two volumes of fibroblast suspension solution (5×10^5 cells/ml in 1×DMEM supplemented with 10% FCS) were added to eight volumes of the collagen solution (the final collagen concentration was 0.8 mg/ml), and then 3.5 ml of the fibroblast-containing collagen solution was applied to each insert. When the fibroblast-containing gel polymerized, DMEM supplemented with 10% FCS and ascorbic acid (final concentration: 50 ng/ml) was added. The gel was kept in submerged culture for 5 days, until the fibroblasts contracted the gel.

Human AM was obtained at cesarean section. Under sterile conditions, the AM was washed with sterile phosphate-buffered saline (PBS) and stored at −80°C in 12% dimethylsufoxide in PBS. Before use, the AM was thawed, washed three times with PBS, and cut into pieces (2.5×2.5 cm). The epithelial cells were removed from the AM by incubation in 0.02% EDTA at 37°C for 2 h and then gentle scraping with a cell scraper under a microscope. The spongy layer was also removed. The complete removal of the epithelial cells was confirmed by using hematoxylin and eosin (HE) staining.

The de-epithelialized AM was put, epithelial side up, onto the contracted gel surface, and a stainless steel ring (interior diameter: 11 mm) was overlaid on it to stabilize it. In the hole of the ring, 4×10^5 keratinocytes in 100 μl MCDB 153 type II were seeded onto the AM. The keratinocytes were maintained, submerged in culture, for 2 days. When the keratinocytes reached confluence, the LSE was lifted to the air-liquid interface and cornification medium (a 1:1 mixture of Ham's F-12 and DMEM supplemented with 2% FCS and other supplements; see Yang et al. 2005) was added. The medium was changed every other day. To construct a conventional LSE, keratinocytes were seeded onto the contracted gel and then submerged and airlifted as described above, except for the use of de-epithelialized AM. The stainless steel rings were used to adjust the seeding cell density. Both types of LSE were harvested 7 and 21 days after airlifting. For HE staining, the LSE was fixed in 20% formalin and embedded in paraffin. For immunohistochemical staining, the LSE was snap-frozen in OCT compound. We performed more than 20 experiments, with similar results being obtained in each (a representative experiment is shown in the figures). In comparative studies, keratinocytes and fibroblasts from the same donor were used.

Histology and immunohistochemical staining

Paraffin-embedded LSE samples were sectioned at 6 μm and stained with HE. For immunohistochemical staining, a Histofine Simple Stain MAX-PO (M) kit (Nichirei, Tokyo, Japan) was used according to the manufacturer's instructions. Frozen sections (7 μm) were first incubated with 0.3% hydrogen peroxide for 30 min to remove endogenous peroxidase activity and then incubated with primary antibodies at appropriate dilutions (Table 1) overnight at 4°C. The sections were incubated with enzyme-conjugated

secondary antibodies for 30 min at room temperature and then with the staining substrate. Images were obtained by using an Olympus AX80 microscope coupled with an Olympus DP50 digital camera (Olympus, Tokyo, Japan). We performed at least three independent studies and obtained similar results (a representative experiment is shown in the figures).

Evaluating the epidermal spreading potential of AM-LSEs

Stainless steel rings with an inner diameter of 6 mm were put on gels with or without AM, and 2×10^5 keratinocytes in 30 µl of MCDB 153 II medium were seeded in the hole of each ring. When the keratinocytes reached confluence, the LSEs were lifted to the air-liquid surface, and the stainless steel rings were removed. At days 0, 3, 5, 7, and 10 after being airlifted, epidermal size was measured by using a computer-assisted morphometric analysis. The epidermal size of the conventional and AM-LSEs was compared statistically by using Student's *t*-test.

Transplanting cultured LSEs

The animal grafting protocol was approved by the Ethics Committee of Ehime University School of Medicine. Eight-week-old female BALB/cAJc1-nu nude mice were anesthetized by intraperitoneal injection of 0.3 ml of Avertin (1.25% tribromoethanol, 2.5% 2-methyl-2-butanol solution). Full-thickness wounds were created on the skin of the backs of each mouse by using an 8-mm skin biopsy punch. A piece of AM-LSE or conventional LSE of matching size (7 days after airlift) obtained using the same punch was grafted onto the wound and covered with a transparent film. At 14 days after transplantation, the grafts were harvested. One part of each graft was paraffin-embedded and sectioned at 6 µm. Some sections were stained with HE, and some were de-paraffinized and blocked for endogenous peroxidase activity and then blood vessels were stained with rabbit antibody against type IV collagen (at dilution 1:50; American Research Products, Belmont, Mass.) according to the protocol of the Histofine SAB-AP (R) kit (Nichirei, Tokyo, Japan). Finally, the sections were counterstained with hematoxylin for cell nuclei. One part of each graft was also processed for electron-microscopic analysis. We performed at least three independent studies and obtained similar results (a representative experiment is shown in the figures).

Transmission electron microscopy

Specimens were fixed with 0.1% tannic acid, 2.5% glutaraldehyde in 0.1 M phosphate buffer (pH 7.4) for 2 h, washed with phosphate buffer, postfixed with 1% osmium tetroxide in phosphate buffer for 2 h, washed with 0.25 M sucrose solution, dehydrated in a graded series of ethanol, and embedded in an Epon-resin mixture. Ultrathin sections (<60–80 nm) were prepared by using a Leica Ultracut S, double-stained with uranyl acetate and lead citrate, and examined with a transmission electron microscope (JEM-1230, JEOL, Tokyo, Japan) at 80 kV.

Results

AM-LSE has a better-organized and more mature epidermis

Both AM-LSE and the conventional LSE showed differentiated epidermis with a basal layer, suprabasal layer, and stratum corneum at days 7 and 21 after airlifting (Fig. 1). The epidermal stratification was however better organized in the AM-LSE; the basal cells were cuboid, smaller, and more compact, and aligned along the AM with clear demarcation (Fig. 1a,b). In the conventional LSE, the epidermal stratification was not as well organized. The larger round basal cells were sparsely aligned along the dermal-epidermal junction, and the number of basal cells had decreased considerably by day 21 (Fig. 1e,f).

We found keratin 6, a marker of keratinocyte activation, only in hair follicles in normal human skin sections (Fig. 2). In AM-LSE, keratin 6 staining was faint at day 7 and disappeared almost completely in the basal and lower suprabasal layers by day 21 (Fig. 2a,k). In conventional LSE, the epidermis strongly expressed keratin 6 up to

Table 1 Details of primary antibodies used

Antigen	Clone	Dilution of antibody	Antibody source
E-cadherin	HECD-1	1:100	TaKaRa
Desmoglein 1	27B2	1:100	Zymed
Desmoglein 3	5G11	1:100	Zymed
Keratin 10	LHP1	1:100	NeoMarkers
Keratin 6	LHK6B	1:100	NeoMarkers
Integrin β4	3E1	1:100	Chemicon
Integrin α6	6B4	1:100	Chemicon
Collagen VII	LH7:2	1:100	NeoMarkers
Collagen IV	2311C3	1:200	Chemicon
Laminin 5	GB3	1:100	Sera-lab

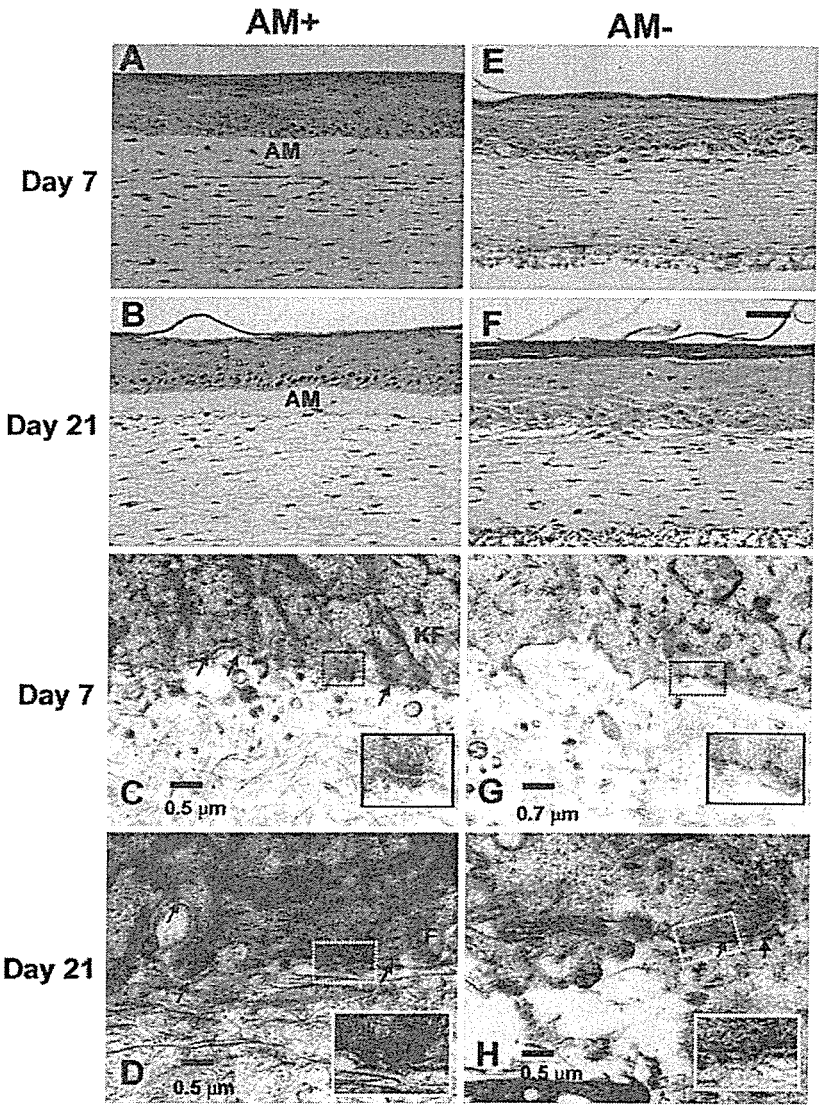

Fig. 1 Morphology of the epidermis and basement membrane (BM) in living skin-equivalent derived from amniotic membrane (AM-LSE; *AM+*) and in conventional LSE (*AM−*). Samples were harvested at days 7 (**a**, **e**, **c**, **g**) and 21 (**b**, **f**, **d**, **h**) from AM-LSE (**a**, **b**, **c**, **d**) and conventional LSE (**e**, **f**, **g**, **h**). Hematoxylin and eosin (HE) staining (**a**, **b**, **e**, **f**) showed a better-stratified epidermis with more compact, columnar basal cells in AM-LSEs. Transmission electron microscopy (**c**, **d**, **g**, **h**) revealed a more continuous lamina densa (*arrows*) and better-developed hemidesmosomes (*insets*) in the AM-LSEs than in the conventional LSEs (*KF* keratin filaments). *Bars* 50 μm (**a**, **b**, **e**, **f**), 0.5 μm (**c**, **d**, **h**), 0.7 μm (**g**)

day 21 after airlifting (Fig. 2f,p). In AM-LSE, keratin 10 expression increased with time, and by day 21, keratin 10 was distributed from the suprabasal layer to the stratum corneum, in a pattern similar to that of normal human skin (Fig. 2b,l). By contrast, keratin 10 expression decreased at day 7 and was barely observed at day 21 in the conventional LSE (Fig. 2g,q). In both LSE models, cell-cell junctions were well developed in similar patterns, as documented by the strongly expressed cell-cell junction proteins, such as E-cadherin (Fig. 2c,h,m,r), desmoglein 1 (Fig. 2d,i,n,s), and desmoglein 3 (Fig. 2e,j,o,t).

Presence of de-epithelialized AM enhances development of BM and hemidesmosomes in LSE

Types IV and VII collagen were present in de-epithelialized AM (data not shown). In the AM-LSE, immunohistochemical staining for types IV and VII collagen was seen along the epidermal-dermal junction at 7 days after airlifting (Fig. 3a,b). The type IV collagen staining was more intense at day 21 (Fig. 3k), whereas less collagen VII was observed (Fig. 3l). In conventional LSE at day 7, only small amounts of collagen IV and VII were noted along the epidermal-dermal junction (Fig. 3f,g), and although the staining increased, it still appeared minimal at day 21 (Fig. 3p,q).

The assembly of the BM was also characterized by determining the distribution of laminin 5 and its receptor, α6β4 integrin. BM normalization could be assessed by the degree to which these proteins were deposited in a polarized linear pattern at the BM zone (Andriani et al. 2003). In AM-LSE, laminin 5 was deposited linearly and was polarized along the epidermal-dermal junction at day 7 (Fig. 3c); the staining intensity had increased by day 21 (Fig. 3m). By contrast, in conventional LSE, little laminin 5 was seen at day 7 (Fig. 3h); by day 21, although more laminin 5 was expressed, its localization was discontinuous and patchy at the suprabasal layer (Fig. 3r). The receptor, α6β4 integrin, was distributed in a pattern similar to that of

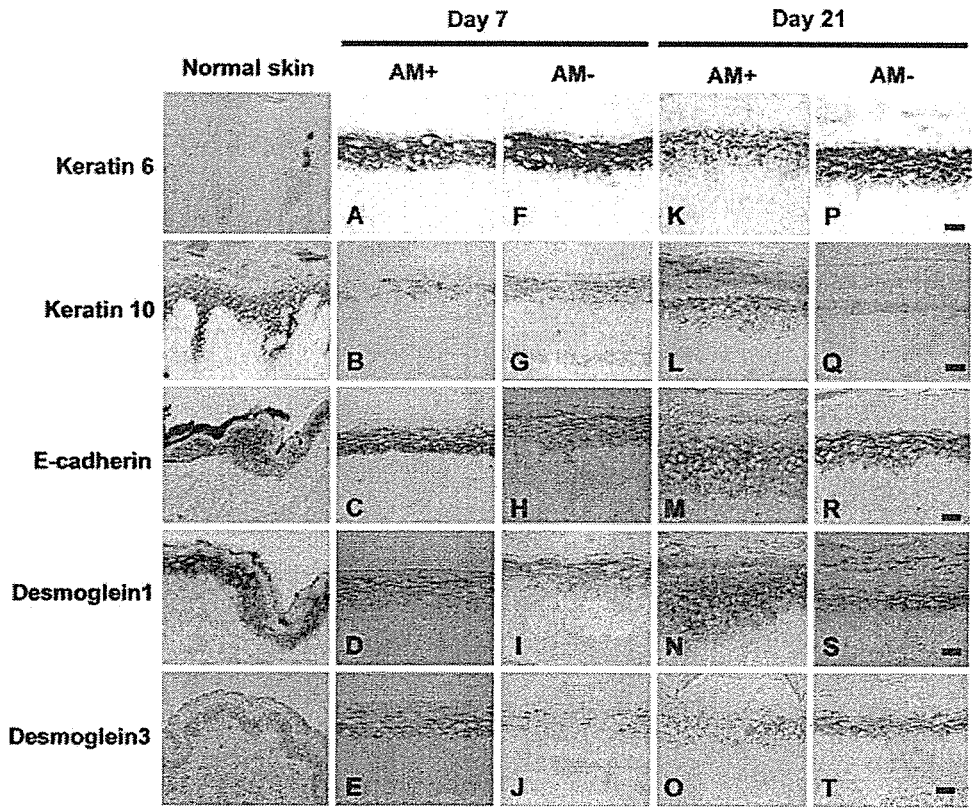

Fig. 2 Keratin and cell-cell junction protein expression in AM-LSE (*AM+*) and conventional LSE (*AM−*). Samples from days 7 (**a-j**) and 21 (**k-t**) from AM-LSEs (**a-e**, **e-o**) and conventional LSEs (**f-j**, **p-t**) were processed for immunohistochemical analysis. The expression of keratin 6 (**a**, **f**, **k**, **p**), keratin 10 (**b**, **g**, **l**, **q**), E-cadherin (**c**, **h**, **m**, **r**), desmoglein 1 (**d**, **i**, **n**, **s**), and desmoglein 3 (**e**, **j**, **o**, **t**) was determined by using the respective monoclonal antibodies. *Bars* 50 μm

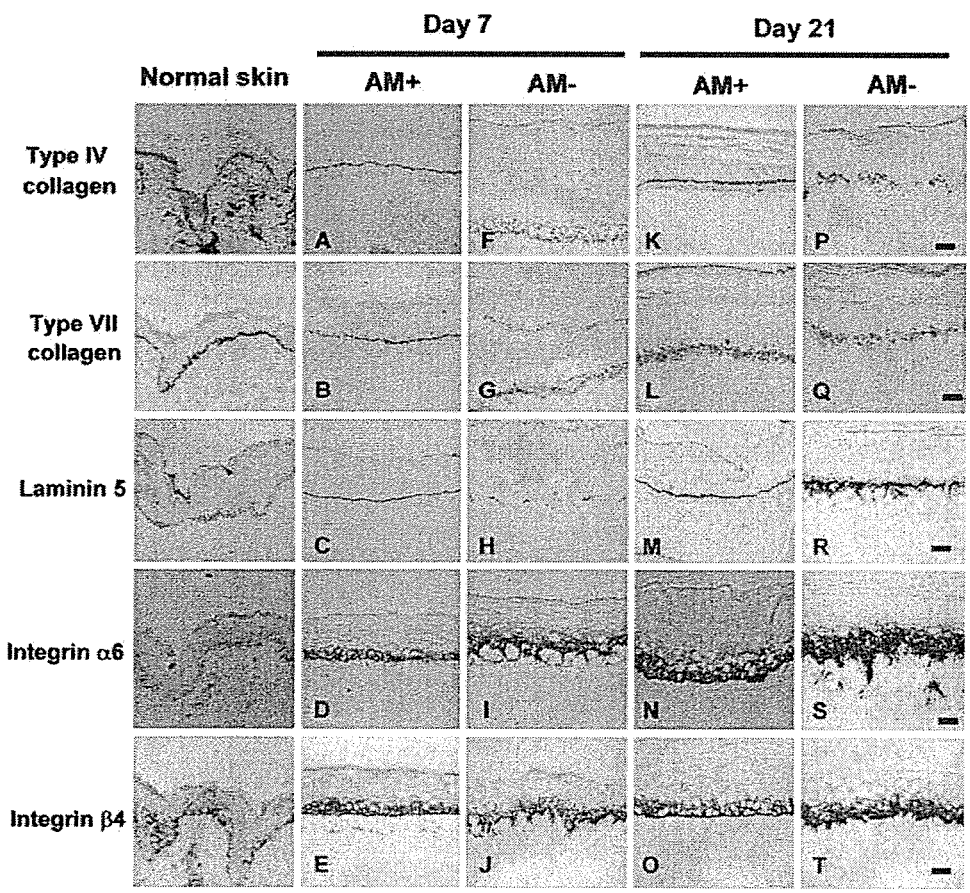

Fig. 3 Integrin and BM component expression in AM-LSE (*AM+*) and conventional LSE (*AM−*). Samples of AM-LSE (**a-e**, **k-o**) and conventional LSE (**f-j**, **p-t**) cultured for 7 (**a-j**) or 21 days (**k-t**) were stained immunohistochemically with monoclonal antibodies against type IV collagen (**a**, **f**, **k**, **p**), type VII collagen (**b**, **g**, **l**, **q**), laminin 5 (**c**, **h**, **m**, **r**), integrin α6 (**d**, **i**, **n**, **s**), and integrin β4 (**e**, **j**, **o**, **t**). *Bars* 50 μm

laminin 5. In AM-LSE, both α6 and β4 integrin subunits were restricted to the basal pole of the basal cells at days 7 and 21 (Fig. 3d,n,e,o). In conventional LSE, α6 and β4 integrin proteins were synthesized and accumulated in the epidermis; they were distributed predominantly in the suprabasal layer and did not localize in a linear pattern (Fig. 3i,s,j,t).

The development of the BM zones of the LSEs was further elucidated by using transmission electron microscopy (TEM) (Fig. 1c,d,g,h). At day 7, a continuous lamina densa was formed along the plasma membrane of the keratinocytes, with many hemidesmosomes, in the AM-LSE. The hemidesmosomes were well developed structurally, with inner and outer plaques clearly being distinguished; keratin filaments were connected to the inner plaques (Fig. 1c), whereas in the conventional LSE, little lamina densa or BM structures were seen at day 7. Along the plasma membrane of the basal cells, some electron-dense hemidesmosome-like structures were seen; however, they did not possess the structural features of hemidesmosomes (Fig. 1g). At day 21, the lamina densa and hemidesmosomes in the AM-LSE were well developed, and the structural features of hemidesmosomes were clearly displayed (Fig. 1d), whereas in conventional LSE, an interrupted lamina densa was seen, with poorly developed hemidesmosomes (Fig. 1h).

De-epithelialized AM improved epidermal outgrowth

On the day of airlifting (day 0), the epidermis of both the AM-LSE and conventional LSE was 6 mm in diameter. The epidermis of the AM-LSE continued to outgrow faster than that of the conventional LSE (Fig. 4): at day 3, the epidermis measured 7.7±0.4 mm (it had increased by 28.3%), and at day 10, it reached 18.3±1.1 mm (over three times its original size). By contrast, the epidermis of the conventional LSE did not change in size by day 3, and only a 78.3% increase to 10.7±0.2 mm was seen at day 10. These results indicated that the AM stimulated keratinocyte migration and proliferation.

AM-LSE grafts on nude mice exhibit better morphogenesis of the epidermis and BM

Two weeks after transplantation, the grafts were harvested and manipulated for observation by light microscopy and TEM. Both the AM-LSE and conventional LSE took well on the recipient nude mice. The fibroblast-populated gel in conventional LSE was prone to separate from the epidermis and was fragile during manipulation. The epidermis of the AM-LSE was tightly attached to the underlying tissue, and the graft was more resistant to rupture. The epidermis of both types of graft was well differentiated with a thick stratum corneum (Fig. 5a,b). The epidermis of the AM-LSE was better stratified than that of the conventional LSE, and the basal cells were columnar and aligned on the surface of the AM (Fig. 5a). By contrast, the epidermal

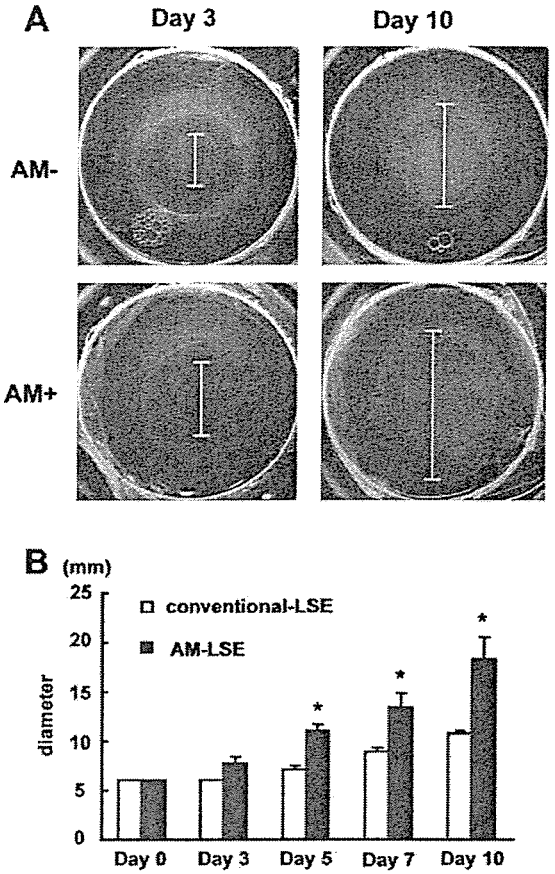

Fig. 4 Comparison of epidermal outgrowth of AM-LSE and conventional LSE. **a** Stainless steel rings with an inner diameter of 6 mm were placed on gels with (*AM+*) or without (*AM−*) AM, and 2×10^5 keratinocytes were seeded. When the keratinocytes reached confluence, the LSEs were lifted to the air-liquid surface, and the stainless steel rings were removed. Epidermal size (*lines*) was monitored after airlifting. **b** The epidermal diameter of AM-LSE and conventional LSE was measured at days 3, 5, 7, and 10, and the mean value for each day was calculated (n=3, *P<0.05)

stratification in the conventional LSE was disorganized, with few basal cells along the dermal-epidermal junction (Fig. 5b).

In the AM- LSE graft, an electron-lucent lamina lucida was clearly observed between the basal cell plasma membrane and the continuous electron-dense lamina densa. Hemidesmosomes were well developed structurally and dotted along the plasma membrane of the basal cells (Fig. 5c). By contrast, the BM in the conventional LSE graft was rudimentary and faint, and far fewer hemidesmosomes were present than in the AM-LSE graft, as seen in vitro (Fig. 5d).

The basal cell number per millimeter in three separate fields of view of both LSE grafts was calculated and showed a significantly higher cell number in AM-LSEs than in conventional LSEs (Fig. 5h). Since vascularization is essential for graft survival, we investigated the angiogenesis in AM-LSE and conventional LSE. We found the AM-LSE grafts were better vascularized, with even some capillaries infiltrating into the AM (Fig. 5e), whereas blood

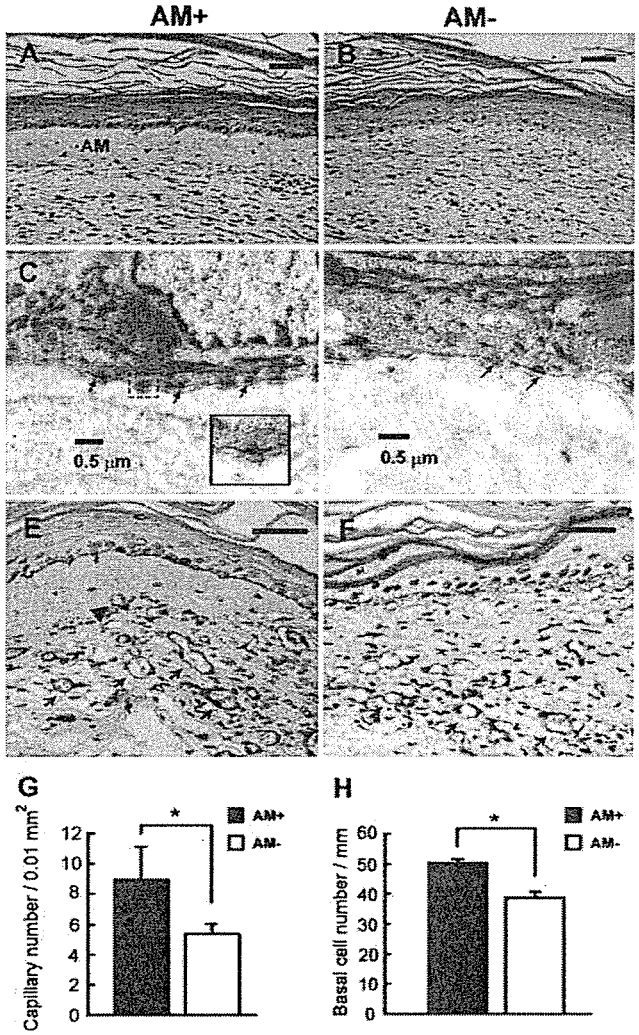

Fig. 5 Light-microscopic and ultrastructural views of AM-LSE (*AM+*) and conventional LSE (*AM−*) in vivo. AM-LSE or conventional LSE was grafted onto the back skin of nude mice. Two weeks after transplantation, samples were harvested and processed for HE staining (**a**, **b**), TEM (**c**, **d**), and immunohistochemical staining for type IV collagen to detect blood vessels (**e**, **f**). HE staining showed better organized epidermis (**a**, **b**) and more basal cells (**h**) in AM-LSE grafts than in conventional LSE grafts. TEM revealed a continuous lamina densa (*arrows* in **c**) with many structurally well-developed hemidesmosomes (*inset* in **c**) in the AM-LSE, and a faint interrupted lamina densa (*arrows* in **d**) with fewer, poorly developed hemidesmosomes in the conventional LSE. More blood vessels (*arrows* in **e**, **f**) were found in AM-LSE grafts than in conventional LSE grafts (**e**, **f**, **g**), with some vessels infiltrating into the AM (*arrowhead* in **e**). $*P<0.05$ (**g**, **h**). *Bars* 50 μm (**a**, **b**, **e**, **f**), 0.5 μm (**c**, **d**)

vessels were fewer in conventional LSE grafts (Fig. 5f). The number of blood vessels/0.01 mm^2 in three separate fields of view was calculated and revealed significantly more blood vessels in AM-LSE grafts than in conventional LSE (Fig. 5g).

Discussion

Epithelial-mesenchymal interactions play important roles in controlling epidermal morphogenesis and homeostasis. The interaction between keratinocytes and the insoluble BM proteins contributes to the maintenance of tissue architecture and affects various biological processes, such as cell attachment, proliferation, differentiation, and migration (Blomme et al. 1998; Kim et al. 1994). In autologous split-thickness skin grafting for treating deep burns, a disturbance in BM reassembly is believed to be responsible for post-burn blisters (Bergman et al. 1997). In conventional LSEs constructed by seeding keratinocytes on a fibroblast-populated type I collagen gel, the BM is not well developed a few weeks after airlifting and is rarely seen after their transplantation onto nude mice (Amano et al. 2001; Medalie et al. 1997).

During the construction of a LSE, pre-existing BM components on the dermal matrix contribute to improving the morphology of the epidermis and are necessary for the formation of hemidesmosomes and the development of a lamina densa (Kim et al. 2001; Medalie et al. 1997; Ralston et al. 1999). The de-epithelialized AM is immunohistochemically positive for types VII and IV collagen, but negative for laminin 5 (data not shown), which is probably lost during the EDTA treatment and subsequent mechanical scraping used to remove epithelial cells from the AM. In this study, we have constructed LSEs with or without de-epithelialized AM to investigate the usefulness of AM. The same types of keratinocytes and fibroblasts and the same techniques have been used for both types of LSE in order to elucidate the roles of de-epithelialized AM in epidermal morphology, BM development, and epidermal migration. We have compared the two types of LSE morphologically, immunohistochemically, and ultrastructurally.

The results indicate that the presence of certain BM components on de-epithelialized AM improve the epidermogenesis of the overlaying epidermis, which is more mature and better organized than epidermis without AM. Similar effects of BM proteins have also been documented in a composite skin-equivalent by using, as the substrate, acellular dermis, which retains several key BM components (Medalie et al. 1997; Ralston et al. 1999). The sustained growth of the keratinocytes in an LSE is maintained by a well-developed BM (Andriani et al. 2003), whose formation is facilitated by the pre-existing BM components.

Laminin 5 is also essential for epidermal-dermal adhesion. Laminin 5 bridges integrin $\alpha6\beta4$ with underlying connective tissue through an association with laminin 6 and 7 and direct binding to type VII collagen (Champliaud et al. 1996; Rousselle et al. 1997). The effect of pre-existing BM components in normalizing the deposition and polarization of laminin 5 has been documented in the construction of LSE by seeding keratinocytes on de-epithelialized dermis (Andriani et al. 2003, 2004). Moreover, the presence of laminin 5 initiates hemidesmosome formation and accelerates the formation of the lamina densa (Nishiyama et al. 2000; Tsunenaga et al. 1998). The de-epithelialized AM

also enhances the polarized basal distribution of α6β4 integrin along the dermal-epidermal junction, as compared with the more suprabasal, albeit denser, distribution in conventional LSEs.

The well-developed basal lamina and hemidesmosomes and the polarized basal deposition of laminin 5 and α6β4 integrin guarantee a stable association between the epidermis and the underlying tissues in AM-LSEs. This might explain why the epidermis is more resistant to separation from the underlying connective tissue during the manipulation of AM-LSEs, as compared with the loose connection in conventional LSEs.

The outgrowth of corneal explants has been reported to be faster on de-epithelialized AM than on intact AM; this implies that the exposed extracellular matrix of de-epithelialized AM is more inducive to epithelial cell migration (Koizumi et al. 2000). Of the BM components, collagen IV had been shown to assist keratinocyte migration through an interaction with keratinocyte α2β1 integrin (Kim et al. 1994). In AM-LSEs, the epidermis outgrows much faster than when on a fibroblast-populated type I collagen gel; AM-LSEs might thus better meet the clinical need to provide a skin-equivalent for a larger area in a shorter time.

AM-LSE therefore appears superior to conventional LSE in several ways (see above). We have transplanted AM-LSE and conventional LSE onto nude mice and found that both LSEs take well on full-thickness wounds of nude mice. A better-organized epidermis, continuous lamina densa and lamina lucida, better-formed hemidesmosomes, and more importantly, better vascularization are seen with AM-LSE. When manipulating the graft for transplantation, the AM-LSE is much more resistant to rupture, as compared with the fragile conventional LSE.

However, the lack of the BM zone in conventional LSE can be supplemented not only by the epidermal side of the de-epithelialized amnion, but also by the stromal side of the amnion, which can support the growth of fibroblasts (Espana et al. 2003; Kumar et al. 2003). This implies that amnion could provide a scaffold for LSE, greatly simplifying the procedures for making dermal matrix and avoiding the use of animal collagen, which is costly and ethically problematic. Moreover, the limited immunogenicity and immune-privilege of amnion (Kubo et al. 2001; Mahgoub et al. 2004), together with its anti-inflammatory effects (Park and Tseng 2000), make it a suitable material for transplantation and a biological immune barrier for xenotransplantation, which may facilitate allograft transplantation of AM-LSE. Amnion can be readily obtained from cesarean delivery under screening for viral diseases and can also be sterilized and preserved at low cost for long periods without obvious architectural changes (Ravishanker et al. 2003; Rejzek et al. 2001; von Versen-Hoynck et al. 2004), thereby ensuring the plentiful supply of amnion in clinical application. Usually, we can take five to six pieces of amnion of 40–50 mm in size in one delivery. Amnion of this size is easily manipulated, fits the commonly used transwell culture insert (diameter: 75 mm), and can be tailored and used in one piece to cover fresh wounds or made into mesh grafts or stamp grafts to cover granulation tissue as split skin grafts.

In conclusion, the AM-LSE had good epidermal morphology and a well-developed BM zone and is easy to manipulate during transplantation. Since AM is readily obtainable, and since a large amount of AM can be supplied compared with other materials, an AM-LSE should be a good skin substitute for treating burns, ulcers, and other skin defects.

Acknowledgements We thank Teruko Tsuda, Eriko Tan, and Wakana Itoh for technical assistance.

References

Amano S, Akutsu N, Matsunaga Y, Nishiyama T, Champliaud MF, Burgeson RE, Adachi E (2001) Importance of balance between extracellular matrix synthesis and degradation in basement membrane formation. Exp Cell Res 271:249–262

Andriani F, Margulis A, Lin N, Griffey S, Garlick JA (2003) Analysis of microenvironmental factors contributing to basement membrane assembly and normalized epidermal phenotype. J Invest Dermatol 120:923–931

Andriani F, Garfield J, Fusenig NE, Garlick JA (2004) Basement membrane proteins promote progression of intraepithelial neoplasia in 3-dimensional models of human stratified epithelium. Int J Cancer 108:348–357

Bergman R, David R, Ramon Y, Ramon M, Kerner H, Kilim S, Peled I, Friedman-Birnbaum R (1997) Delayed postburn blisters: an immunohistochemical and ultrastructural study. J Cutan Pathol 24:429–433

Blomme EA, Weckmann MT, Capen CC, Rosol TJ (1998) Influence of extracellular matrix macromolecules on normal human keratinocyte phenotype and parathyroid hormone-related protein secretion and expression in vitro. Exp Cell Res 238: 204–215

Champliaud MF, Lunstrum GP, Rousselle P, Nishiyama T, Keene DR, Burgeson RE (1996) Human amnion contains a novel laminin variant, laminin 7, which like laminin 6, covalently associates with laminin 5 to promote stable epithelial-stromal attachment. J Cell Biol 132:1189–1198

Eaglstein WH, Falanga V (1998) Tissue engineering and the development of Apligraf a human skin equivalent. Adv Wound Care 11:1–8

Espana EM, He H, Kawakita T, Di Pascuale MA, Raju VK, Liu CY, Tseng SC (2003) Human keratocytes cultured on amniotic membrane stroma preserve morphology and express keratocan. Invest Ophthalmol Vis Sci 44:5136–5141

Guerret S, Govignon E, Hartmann DJ, Ronfard V (2003) Long-term remodeling of a bilayered living human skin equivalent (Apligraf) grafted onto nude mice: immunolocalization of human cells and characterization of extracellular matrix. Wound Repair Regen 11:35–45

Kim JP, Chen JD, Wilke MS, Schall TJ, Woodley DT (1994) Human keratinocyte migration on type IV collagen. Roles of heparin-binding site and alpha 2 beta 1 integrin. Lab Invest 71:401–408

Kim SW, Park KC, Kim HJ, Cho KH, Chung JH, Kim KH, Eun HC, Lee JS, Park KD (2001) Effects of collagen IV and laminin on the reconstruction of human oral mucosa. J Biomed Mater Res 58:108–112

Koizumi N, Fullwood NJ, Bairaktaris G, Inatomi T, Kinoshita S, Quantock AJ (2000) Cultivation of corneal epithelial cells on intact and denuded human amniotic membrane. Invest Ophthalmol Vis Sci 41:2506–2513

Kubo M, Sonoda Y, Muramatsu R, Usui M (2001) Immunogenicity of human amniotic membrane in experimental xenotransplantation. Invest Ophthalmol Vis Sci 42:1539–1546

Kumar TR, Shanmugasundaram N, Babu M (2003) Biocompatible collagen scaffolds from a human amniotic membrane: physicochemical and in vitro culture characteristics. J Biomater Sci Polym Ed 14:689–706

Llames SG, Del Rio M, Larcher F, Garcia E, Garcia M, Escamez MJ, Jorcano JL, Holguin P, Meana A (2004) Human plasma as a dermal scaffold for the generation of a completely autologous bioengineered skin. Transplantation 77:350–355

Mahgoub MA, Ammar A, Fayez M, Edris A, Hazem A, Akl M, Hammam O (2004) Neovascularization of the amniotic membrane as a biological immune barrier. Transplant Proc 36: 1194–1198

Meana A, Iglesias J, Del Rio M, Larcher F, Madrigal B, Fresno MF, Martin C, San Roman F, Tevar F (1998) Large surface of cultured human epithelium obtained on a dermal matrix based on live fibroblast-containing fibrin gels. Burns 24:621–630

Medalie DA, Eming SA, Collins ME, Tompkins RG, Yarmush ML, Morgan JR (1997) Differences in dermal analogs influence subsequent pigmentation, epidermal differentiation, basement membrane, and rete ridge formation of transplanted composite skin grafts. Transplantation 64:454–465

Nakamura T, Endo K, Cooper LJ, Fullwood NJ, Tanifuji N, Tsuzuki M, Koizumi N, Inatomi T, Sano Y, Kinoshita S (2003a) The successful culture and autologous transplantation of rabbit oral mucosal epithelial cells on amniotic membrane. Invest Ophthalmol Vis Sci 44:106–116

Nakamura T, Koizumi N, Tsuzuki M, Inoki K, Sano Y, Sotozono C, Kinoshita S (2003b) Successful regrafting of cultivated corneal epithelium using amniotic membrane as a carrier in severe ocular surface disease. Cornea 22:70–71

Nakamura T, Yoshitani M, Rigby H, Fullwood NJ, Ito W, Inatomi T, Sotozono C, Nakamura T, Shimizu Y, Kinoshita S (2004) Sterilized, freeze-dried amniotic membrane: a useful substrate for ocular surface reconstruction. Invest Ophthalmol Vis Sci 45:93–99

Nishiyama T, Amano S, Tsunenaga M, Kadoya K, Takeda A, Adachi E, Burgeson RE (2000) The importance of laminin 5 in the dermal-epidermal basement membrane. J Dermatol Sci 24: S51–S59

Ojeh NO, Frame JD, Navsaria HA (2001) In vitro characterization of an artificial dermal scaffold. Tissue Eng 7:457–472

Oyama N, Bhogal BS, Carrington P, Gratian MJ, Black MM (2003) Human placental amnion is a novel substrate for detecting autoantibodies in autoimmune bullous diseases by immunoblotting. Br J Dermatol 148:939–944

Park WC, Tseng SC (2000) Modulation of acute inflammation and keratocyte death by suturing, blood, and amniotic membrane in PRK. Invest Ophthalmol Vis Sci 41:2906–2914

Ralston DR, Layton C, Dalley AJ, Boyce SG, Freedlander E, MacNeil S (1999) The requirement for basement membrane antigens in the production of human epidermal/dermal composites in vitro. Br J Dermatol 140:605–615

Ravishanker R, Bath AS, Roy R (2003) "Amnion Bank"—the use of long term glycerol preserved amniotic membranes in the management of superficial and superficial partial thickness burns. Burns 29:369–374

Rejzek A, Weyer F, Eichberger R, Gebhart W (2001) Physical changes of amniotic membranes through glycerolization for the use as an epidermal substitute. Light and electron microscopic studies. Cell Tissue Bank 2:95–102

Rousselle P, Keene DR, Ruggiero F, Champliaud MF, Rest M, Burgeson RE (1997) Laminin 5 binds the NC-1 domain of type VII collagen. J Cell Biol 138:719–728

Sheridan RL, Moreno C (2001) Skin substitutes in burns. Burns 27:92

Shirakata Y, Tokumaru S, Yamasaki K, Sayama K, Hashimoto K (2003) So-called biological dressing effects of cultured epidermal sheets are mediated by the production of EGF family, TGF-beta and VEGF. J Dermatol Sci 32:209–215

Shirakata Y, Ueno H, Hanakawa Y, Kameda K, Yamasaki K, Tokumaru S, Yahata Y, Tohyama M, Sayama K, Hashimoto K (2004) TGF-beta is not involved in early phase growth inhibition of keratinocytes by 1alpha,25(OH)2vitamin D3. J Dermatol Sci 36:41–50

Tseng SC (2001) Amniotic membrane transplantation for ocular surface reconstruction. Biosci Rep 21:481–489

Tsunenaga M, Adachi E, Amano S, Burgeson RE, Nishiyama T (1998) Laminin 5 can promote assembly of the lamina densa in the skin equivalent model. Matrix Biol 17:603–613

von Versen-Hoynck F, Syring C, Bachmann S, Moller DE (2004) The influence of different preservation and sterilisation steps on the histological properties of amnion allografts-light and scanning electron microscopic studies. Cell Tissue Bank 5:45–56

Yang L, Shirakata Y, Tamai K, Dai X, Hanakawa Y, Tokumaru S, Yahata Y, Tohyama M, Shiraishi K, Nagai H, Wang X, Murakami S, Sayama K, Kaneda Y, Hashimoto K (2005) Microbubble-enhanced ultrasound for gene transfer into living skin equivalents. J Dermatol Sci 40:105–114

THE JOURNAL OF BIOLOGICAL CHEMISTRY VOL. 281, NO. 31, pp. 22013–22020, August 4, 2006

Transforming Growth Factor-β-activated Kinase 1 Is Essential for Differentiation and the Prevention of Apoptosis in Epidermis*

Received for publication, February 3, 2006, and in revised form, April 17, 2006 Published, JBC Papers in Press, June 5, 2006, DOI 10.1074/jbc.M601065200

Koji Sayama[‡1], Yasushi Hanakawa[‡], Hiroshi Nagai[‡], Yuji Shirakata[‡], Xiuju Dai[‡], Satoshi Hirakawa[‡], Sho Tokumaru[‡], Mikiko Tohyama[‡], Lujun Yang[‡], Shintaro Sato[§], Akira Shizuo[§], and Koji Hashimoto[‡]

From the [‡]Department of Dermatology, Ehime University School of Medicine, Ehime 791-0295 and the [§]Research Institute for Microbial Disease, Osaka University, Suita 565-0871, Japan

Transforming growth factor-β-activated kinase 1 (TAK1) is a member of the mitogen-activated protein (MAP) kinase family and is an upstream signaling molecule of nuclear factor-κB (NF-κB). Given that NF-κB regulates keratinocyte differentiation and apoptosis, TAK1 may be essential for epidermal functions. To test this, we generated keratinocyte-specific TAK1-deficient mice from *Map3k7*$^{flox/flox}$ mice and *K5-Cre* mice. The keratinocyte-specific TAK1-deficient mice were macroscopically indistinguishable from their littermates until postnatal day 2 or 3, when the skin started to roughen and wrinkle. This phenotype progressed, and the mice died by postnatal day 7. Histological analysis showed thickening of the epidermis with foci of keratinocyte apoptosis and intra-epidermal micro-abscesses. Immunohistochemical analysis showed that the suprabasal keratinocytes of the TAK1-deficient epidermis expressed keratin 5 and keratin 14, which are normally confined to the basal layer. The expression of keratin 1, keratin 10, and loricrin, which are markers for the suprabasal and late phase differentiation of the epidermis, was absent from the TAK1-deficient epidermis. Furthermore, the TAK1-deficient epidermis expressed keratin 16 and had an increased number of Ki67-positive cells. These data indicate that TAK1 deficiency in keratinocytes results in abnormal differentiation, increased proliferation, and apoptosis in the epidermis. However, the keratinocytes from the TAK1-deficient epidermis induced keratin 1 in suspension culture, indicating that the TAK1-deficient keratinocytes retain the ability to differentiate. Moreover, the removal of TAK1 from cultured keratinocytes of *Map3k7*$^{flox/flox}$ mice resulted in apoptosis, indicating that TAK1 is essential for preventing apoptosis. In conclusion, TAK1 is essential in the regulation of keratinocyte growth, differentiation, and apoptosis.

The epidermis is a multilayered epithelial tissue, maintained by the precise regulation of keratinocyte proliferation, differentiation, and cell death. Cell growth is limited to the basal cell layer, which attaches to the basement membrane. After leaving the basement membrane, keratinocytes differentiate and form a multilayered epidermis instead of undergoing apoptosis. This keratinocyte differentiation is regulated by intracellular signaling pathways involving nuclear factor-κB (NF-κB),[2] the MAP kinase family, phosphatidylinositol 3-kinase, and protein kinase C (1–3).

In the epidermis, NF-κB is found in the cytoplasm of basal cells (1). The functional blockade of NF-κB by expressing dominant negative NF-κB in transgenic mouse epidermis produced a hyperplastic epithelium *in vivo* (1). With deficiency of the p65/RelA subunit of NF-κB, the epidermis is hyperplastic (4). Conversely, the overexpression of active p50 (a subunit of NF-κB) and p65 in the transgenic epithelium produced hypoplasia and growth inhibition, suggesting a role for NF-κB in negative cellular growth control (1). Furthermore, the expression of active p50 and p65 in keratinocytes inhibits cell cycle progression to G_1 arrest *in vitro*, which was associated with an increased p21 level (5) and CDK4 down-regulation (6). This CDK4 regulation is dependent on both the TNFR1 and JNK pathways (7). In addition to regulating differentiation and cell growth, NF-κB protects keratinocytes from apoptosis, and the blockade of NF-κB function in the epidermis by the expression of the dominant negative mutant IκBα provoked premature spontaneous cell death (8). Although the roles of the NF-κB pathway have been studied in keratinocytes, the upstream signal of the NF-κB pathway has not been clarified fully.

Transforming growth factor-β-activated kinase 1 (TAK1), a member of the MAP kinase kinase kinase family, is a signaling molecule upstream from NF-κB and is encoded by the *Map3k7* gene. TAK1 was originally identified as a signaling molecule activated by transforming growth factor β (9). TAK1 is also involved in IL-1 signaling and TNF-α-induced activation of NF-κB and MAP kinases (MAPKs). Activated TAK1 is recruited to TRAF6 and TRAF2, in response to the IL-1 and TNF receptors, respectively (10–12). TAK1 forms a complex

* This work was supported by grants from the Ministries of Health, Labor, and Welfare and Education, Culture, Sports, Science, and Technology of Japan. The costs of publication of this article were defrayed in part by the payment of page charges. This article must therefore be hereby marked "*advertisement*" in accordance with 18 U.S.C. Section 1734 solely to indicate this fact.

[1] To whom correspondence should be addressed: Dept. of Dermatology, Ehime University School of Medicine, Toon, Ehime, 791-0295, Japan. Tel.: 81-89-960-5350; Fax: 81-89-960-5350; E-mail: sayama@m.ehime-u.ac.jp.

[2] The abbreviations used are: NF-κB, nuclear factor-κB; TAK1, transforming growth factor-β-activated kinase 1; MAP, mitogen-activated protein; MAPK, MAP kinase; IKK, IκB kinase; KO, knock-out; K, keratin; Ax, adenovirus vector; P, postnatal day; TAB, TAK1-binding protein; TEWL, trans-epidermal water loss; TUNEL, TdT-mediated dUTP nick end-labeling; RT, reverse transcriptase; JNK, c-Jun NH_2-terminal kinase; IL, interleukin; TNF, tumor necrosis factor; poly-HEMA, polyhydroxyethylmethacrylate; LDH, lactate dehydrogenase.

with TAK1-binding protein (TAB) 1, TAB2, and TAB3 (10, 12–14). The activated TAK1 complex phosphorylates IκB kinases (IKKs) and MAPK kinase 6, which activate NF-κB and MAPKs, respectively. The transfection of TAK1 small interfering RNA markedly inhibited TNF-α- and IL-1-mediated activation of NF-κB (11). Recently, TAK1 was shown to be essential for innate and adaptive immune responses by generating B cell-specific TAK1 deficiency (15).

Given that TAK1 is an upstream signaling molecule of the NF-κB pathway, TAK1 might regulate keratinocyte growth, differentiation, and apoptosis. However, the function of TAK1 in epidermal keratinocytes has not been studied. To address this issue, we generated keratinocyte-specific TAK1-deficient mice by using Cre-recombinase transgenic mice under the control of the K5 promoter.

EXPERIMENTAL PROCEDURES

Generation of Keratinocyte-specific TAK1-deficient Mice Using Gene Targeting with the Cre Transgene—The targeting construct has been described previously (15). We generated keratinocyte-specific TAK1-deficient mice by breeding *Map3k7*$^{flox/flox}$ mice with mice carrying the *Cre* transgene under the control of the keratin 5 promoter (*K5-Cre*) (16). The *Map3k7*$^{flox/flox}$ mice were bred with *K5-Cre* mice to generate *K5-Cre/Map3k7*$^{flox/+}$ mice. Subsequently, the *K5-Cre/Map3k7*$^{flox/+}$ mice were bred to *Map3k7*$^{flox/flox}$ mice to generate *K5-Cre/Map3k7*$^{flox/flox}$ mice. The genotype of each mouse was confirmed using PCR and Western blot analysis. The TAK1 primer sequences were 5′-GGAACCCGTGGATAAGTGCACTTGAAT-3′ and 5′-GGCTTTCATTGTGGAGGTAAGCTGAGA-3′. The amplified products were 320 bp for the floxed allele and 280 bp for the wild-type allele. The Cre-recombinase primers were 5′-TTACCGGTCGATGCAACGAGTGATG-3′ and 5′-TTCCATGAGTGAACGAACCTGGTCG-3′. Isolated keratinocytes were cultured overnight, and the adherent keratinocytes were harvested for Western blot analysis (see Fig. 1*D*). This protocol was approved by the Institutional Review Board of Ehime University School of Medicine.

Trans-epidermal Water Loss (TEWL)—TEWL was measured using a Tewameter TM210 (Integral Co., Tokyo, Japan) according to the manufacturer's instructions. The data are expressed as the means ± S.E. The statistical significance was determined using the paired Student's *t* test. The differences were considered statistically significant at $p < 0.01$.

Histological Analysis—Mouse skin was fixed in 3.6% formaldehyde, dehydrated, and embedded in paraffin. Four-μm sections were stained with hematoxylin and eosin.

To analyze differentiation markers, keratin (K) 5, K14, K1, K10, and loricrin, the paraffin-embedded sections were deparaffinized, blocked with 10% goat serum, and reacted with the first antibodies overnight at 4 °C. After washing with phosphate-buffered saline, the first antibodies were detected using a peroxidase staining kit (ImmPRESS; Vector Laboratories, Burlingame, CA) and visualized with the chromogen 3-amino-9-ethyl-cabazole according to the manufacturer's instructions. For K16 and Ki67 staining, the deparaffinized sections were boiled in 10 mM citrate buffer, pH 6.0, for 40 min and cooled at room temperature for 20 min for antigen retrieval. Subsequently, K16 and Ki67 were stained following the same procedure as for the differentiation markers.

Confocal Laser Scanning Microscopy—Frozen skin sections (4 μm) were blocked with 10% goat serum and reacted overnight at 4 °C with rabbit anti p50 and p65. After washing with phosphate-buffered saline, the sections were incubated with Alexa Fluor 488-conjugated donkey anti-rabbit IgG for 30 min at room temperature. The stained specimens were observed under a LSM 510 microscope (Carl Zeiss, Jena, Germany). The images were captured using LSM 510 software.

TdT-mediated dUTP Nick End Labeling (TUNEL)—Keratinocyte apoptosis was detected by the TUNEL method using an *in situ* cell death detection kit (Roche Applied Sciences). After being deparaffinized, the sections were treated with 20 μg/ml proteinase K in 10 mM Tris-HCl, pH 7.4, for 15 min at room temperature and labeled according to the manufacturer's instructions. The labeled cells were observed under a fluorescence microscope.

Antibodies—The following antibodies were used: K5, K14, K1, and K10 (rabbit; Covance, Berkeley, CA); K16 (mouse, clone number LL025; Chemicon International, Temecula, CA); loricrin (rabbit; Covance); Ki67 (mouse, clone number MM1, Novo Castra Laboratories, Newcastle, UK); β-actin (mouse, clone number AC-15, Abcam, Cambridge, UK); and p50, p65, and TAK1 (rabbit, Santa Cruz Biotechnology, Santa Cruz, CA).

Keratinocyte Culture—Primary mouse keratinocytes were isolated from newborn mouse skin. The skin samples were cut into 3–5-mm pieces and incubated with 250 units/ml dispase (Godoshusei, Tokyo, Japan) in Dulbecco's modified Eagle's medium overnight at 4 °C. After the epidermis was separated from the dermis, the epidermal sheets were incubated in a 0.25% trypsin solution for 10 min at 37 °C and teased with forceps. The keratinocytes were collected by centrifugation and were cultured further in CnT-02 medium (CellnTec, Bern, Switzerland).

For suspension culture, keratinocytes were plated onto 6-cm polyhydroxyethylmethacrylate (poly-HEMA)-coated plates (3). The poly-HEMA-coated plates were made by adding 4 ml of a solution containing 10 mg/ml poly-HEMA (Sigma-Aldrich) in ethanol to the dish, drying, and repeating once, followed by extensive phosphate-buffered saline washes. After 24 h, the cells were harvested by pipetting.

Western Blotting—Keratinocytes were harvested on ice with lysis buffer containing 1.0% Nonidet P-40, 1% sodium deoxycholate, 0.1% SDS, 150 mM NaCl, 20 mM Tris-HCl, pH 7.5, 1 mM EDTA, and 0.1% protease inhibitor (Sigma-Aldrich). The proteins (20 μg) were separated by 10% SDS-PAGE and transferred to a nitrocellulose membrane. The membrane was blocked with 5% nonfat dry milk in Tris-HCl, pH 7.4, 0.15 M NaCl, and 0.05% Tween 20 and was incubated with the appropriate first antibody. After washing, the membrane was incubated with fluorescein-labeled goat anti-mouse IgG (1:2,500 dilution) for 1 h. The signal was amplified with an anti-fluorescein antibody conjugated with alkaline phosphatase, followed by the fluorescent substrate AttoPhos (Molecular Dynamics, Sunnyvale, CA). The membrane was scanned using FluorImager (Molecular Dynamics),

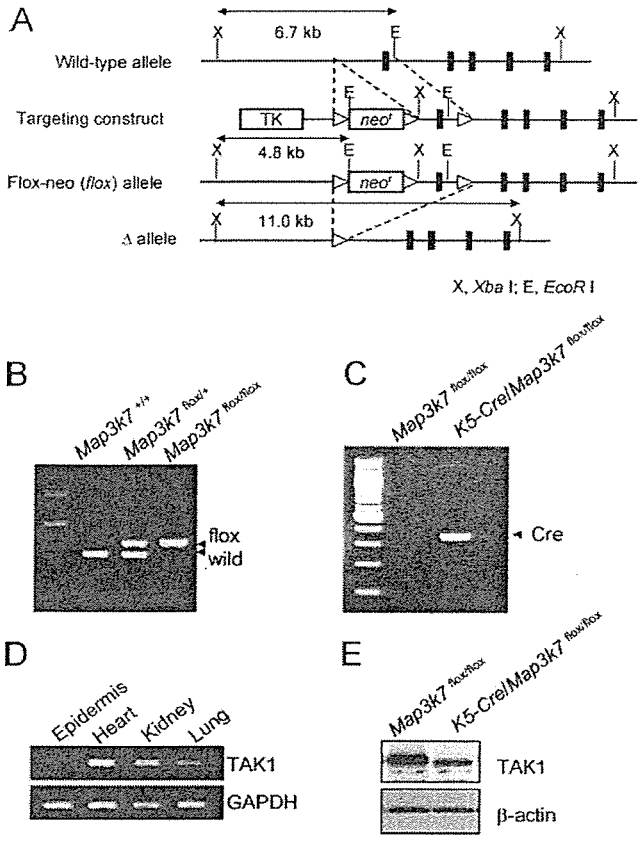

FIGURE 1. **Establishment of mice with keratinocyte-specific TAK1 deficiency.** Keratinocyte-specific TAK1-deficient mice were generated by breeding *Map3k7*$^{flox/flox}$ mice with mice carrying the *Cre* transgene under the control of the keratin 5 promoter (*K5-Cre*) (16). *A*, schematic representation of the targeting strategy. A targeting construct was designed to flank exon 2 of the *Map3k7* gene and the *neo*^{r} gene with *loxP* sites (*triangles*). Cre-mediated removal was performed to generate the deleted (Δ) allele of *Map3k7*. The genotype of each mouse was confirmed by PCR (*B* and *C*). *B*, a primer pair was designed to include the *LoxP* site (*triangle*), so that the PCR products represent the floxed (320 bp) and wild-type (280 bp) alleles of *Map3k7*. *C*, the PCR product represents Cre-recombinase. *D*, RT-PCR analysis showed the *Cre*-mediated keratinocyte-specific deletion of TAK1 in *K5-Cre/Map3k7*$^{flox/flox}$ mice. mRNA isolated from the epidermis, heart, kidney, and lung of *K5-Cre/Map3k7*$^{flox/flox}$ mice at birth was subjected to RT-PCR to determine TAK1 expression. The faint band from the epidermis detected at the expected size is likely the result of the presence of nonkeratinocyte cells in the epidermis, such as Langerhans cells or melanocytes. Glyceraldehyde-3-phosphate dehydrogenase is an internal standard. *E*, Western blot analysis showed the *Cre*-mediated deletion of TAK1 from the keratinocytes of *K5-Cre/Map3k7*$^{flox/flox}$ mice. Keratinocytes isolated from *Map3k7*$^{flox/flox}$ and *K5-Cre/Map3k7*$^{flox/flox}$ mice at birth were subjected to Western blot analysis to detect TAK1. There was a faint band in the keratinocytes from *K5-Cre/Map3k7*$^{flox/flox}$ mice, which was slightly lower than that for *Map3k7*$^{flox/flox}$ mice. This may represent TAK1Δ (*A*), which lacks the ATP-binding site required for kinase activity (15). β-Actin is an internal standard. In this manuscript, *K5-Cre/Map3k7*$^{flox/flox}$ mice and *Map3k7*$^{flox/flox}$ mice are referred as TAK1-KO and control mice, respectively.

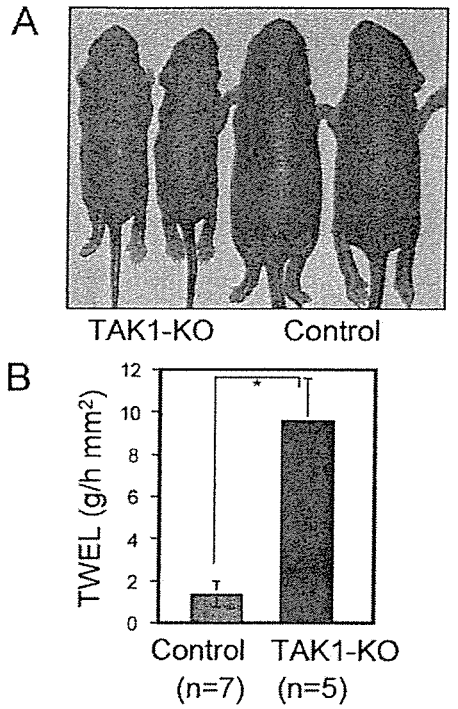

FIGURE 2. **The macroscopic phenotype of TAK1-KO mice.** *A*, appearance of TAK1-KO mice at P6. The skin is rough and wrinkled, with mild scaling. The TAK1-KO mice weighed approximately half the control weight. *B*, TEWL in TAK1-KO mice at P6. The TEWL value, a measure of epidermal barrier function, in TAK1-KO mice ($n = 5$) was 6.9-fold that in the control mouse ($n = 7$). The data are expressed as the means ± S.E. The statistical significance was determined using the paired Student's *t* test. * The difference was considered statistically significant at $p < 0.01$.

and the intensity of each band was quantified with ImageQuant (Molecular Dynamics), referring to the control as one unit.

Reverse Transcriptase (RT)-PCR—Total RNA samples were isolated using Isogen (Nippon Gene, Tokyo, Japan), and the TAK1 mRNA expression was analyzed by RT-PCR using RT-PCR High Plus (Toyobo, Osaka, Japan). The PCR product (337 bp) was sequenced to confirm the accuracy of amplification. The primer sequences for TAK1 were 5′-AGTGCTGACATG-TCTGAAAT-3′ and 5′-TTCGAACACTGCCATGGATT-3′, and those for the internal standard glyceraldehyde-3-phosphate dehydrogenase were 5′-ACCACAGTCCATGCCAT-CAC-3′ and 5′-TCCACCACCCTGTTGCTGTA-3′. The intensity of each band was quantified using NIH Image. The data are presented as fold induction relative to the control signal, set at 1 unit.

Adenovirus Vector—Adenovirus vector (Ax) encoding Cre-recombinase was generated using the COS-TPC method (17). Virus stocks were prepared by standard procedures. Concentrated, purified virus stocks were prepared using a CsCl gradient, and the virus titer was checked using a plaque formation assay. We infected keratinocytes with Ax at a multiplicity of infection of 100. Empty Ax-1W vector was used as a control.

LDH Assay—Cell death was analyzed quantitatively by measuring LDH release using an LDH assay kit (Kyokutokogyo, Tokyo, Japan). Keratinocytes were cultured on 6-cm dishes, and Ax was transfected. At the indicated time, 100 μl of supernatant were harvested, centrifuged, and stored at −70 °C until the LDH assay was performed according to the manufacturer's instructions. The LDH of living cells was obtained by cell lysis with 0.1% Tween 20®. LDH release was expressed as a percentage of the total LDH, which was obtained by summing the LDH released and the LDH of living cells. The data are expressed as the means ± S.E. The statistical significance was determined using the paired Student's *t* test ($n = 5$). The differences were considered statistically significant at $p < 0.01$.

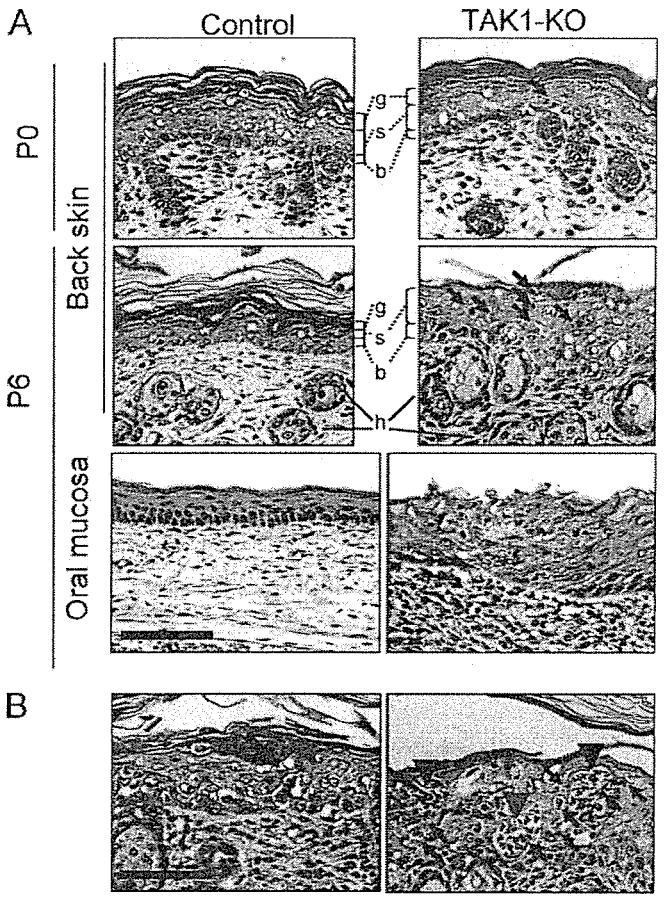

FIGURE 3. **Hyperplasia, apoptosis, and micro-abscesses in the epidermis of TAK1-KO mice.** *A*, histological analysis of TAK1-KO mouse skin at P0 and P6, using hematoxylin and eosin staining. Normal epidermis consists of granular (*g*), spinous (*s*), and basal cell (*b*) layers. *h* indicates a hair follicle in the dermis. TAK1-KO mice at P6 showed marked thickening of the epidermis with no granular layer, and apoptosis (*arrow*). The oral mucosa showed a phenotype similar to that of the epidermis. *B*, the thickened epidermis of TAK1-KO mice contains foci of keratinocyte apoptosis (*left panel, arrow*) and intra-epidermal micro-abscesses (*right panel, arrowhead*), which were associated with apoptotic cells (*arrow*). *Scale bar*, 20 μm.

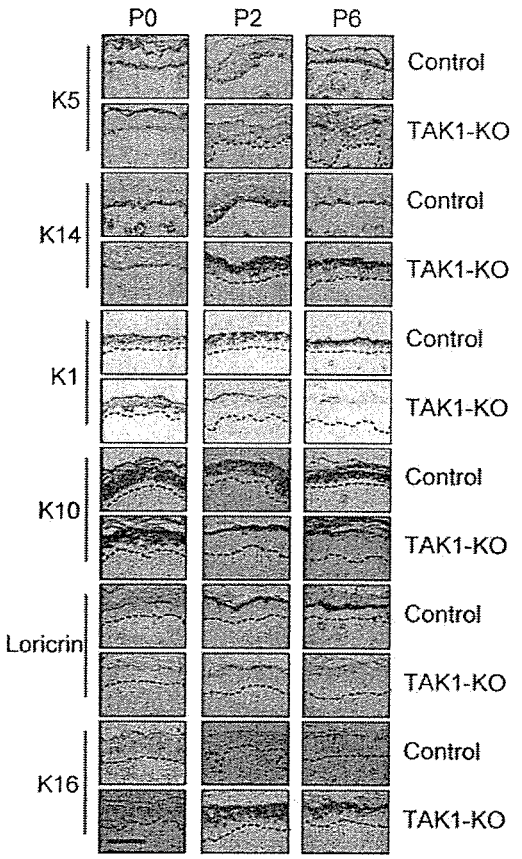

FIGURE 4. **Abnormal expression of differentiation markers in the epidermis of TAK1-KO mice.** Paraffin-embedded skin sections from TAK1-KO mice at P0, P2, and P7 were stained immunohistochemically with antibodies against K5, K14, K1, K10, loricrin, and K16. The expression of K5 and K14 is normally confined to the basal cell layer. The expression of K1, K10, and loricrin marks the suprabasal and late-phase differentiation. K16 is a marker for inflammatory and hyperproliferative epidermal keratinocytes. The *dotted lines* indicate the basement membrane. *Scale bar*, 30 μm.

RESULTS

Generating Mice with Keratinocyte-specific TAK1 Deficiency—The germ line targeting of the *Map3k7* gene encoding TAK1 results in embryonic lethality (15); therefore, we generated keratinocyte-specific TAK1-deficient mice (Fig. 1) by breeding *Map3k7*$^{flox/flox}$ mice with mice carrying the *Cre* transgene under the control of the keratin 5 promoter (*K5-Cre*) (16). Western blot analysis and RT-PCR showed the *Cre*-mediated deletion of TAK1 in keratinocytes from *K5-Cre*/*Map3k7*$^{flox/flox}$ mice at birth (Fig. 1, *D* and *E*). Here, the *K5-Cre*/*Map3k7*$^{flox/flox}$ mice and *Map3k7*$^{flox/flox}$ mice are referred to as TAK1-KO and control, respectively.

Rough and Wrinkled Skin with Disrupted Barrier Function, Growth Retardation, and Early Mortality in TAK1-KO Mice—At birth, the TAK1-KO mice were macroscopically indistinguishable from their littermates until postnatal day 2 or 3 (P2–P3), when the skin started to roughen and wrinkle. This phenotype progressed with mild scaling, and the TAK1-KO mice subsequently died by P7 (Fig. 2*A*). At this stage, the mice weighed approximately half the control weight. To evaluate epidermal barrier function, we measured TEWL at P6 (Fig. 2*B*). The TEWL value in TAK1-KO mice was 6.9-fold that in the control, indicating that the barrier function had been disrupted. Given that the epidermal barrier function arises during keratinocyte differentiation, the regulation of keratinocyte differentiation might be disturbed in TAK1-KO mice. The *Map3k7*$^{flox/+}$ and *Map3k7*$^{+/+}$ mice with or without *K5-Cre* showed no pathological phenotypes.

Hyperplasia, Apoptosis, and Micro-abscess Formation in the Epidermis of TAK1-KO Mice—The epidermis of TAK1-KO mice at P0 was histologically indistinguishable from that of control mice, except for a few apoptotic cells (*arrow*). However, the histological analysis of the skin of TAK1-KO mice at P6 (Fig. 3*A*) showed many apoptotic cells (*arrow*) and marked thickening of the epidermis without a granular layer (*g*), indicating abnormal epidermal differentiation. The thickened epidermis contained foci of keratinocyte apoptosis (Fig. 3*B*, *left panel, arrow*) and intra-epidermal micro-abscesses (Fig. 3*B*, *right panel, arrowhead*), which were associated with apoptotic cells (*arrow*). The oral mucosa showed a similar phenotype to that of the epidermis (Fig. 3*A*). Clinically, there were no apparent erosions or ulcers on the oral mucosa (data not shown).